© 2015. Published by The Company of Biologists Ltd | Development (2015) 142, 510-521 doi:10.1242/dev.115980

RESEARCH ARTICLE

DNA hypomethylation induces a DNA replication-associated cell cycle arrest to block hepatic outgrowth in *uhrf1* mutant zebrafish embryos

Vinitha Jacob[1,2,3], Yelena Chernyavskaya[1,2], Xintong Chen[1,4], Poh Seng Tan[1,4,5], Brandon Kent[1,2,3], Yujin Hoshida[1,3,4] and Kirsten C. Sadler[1,2,3,*]

ABSTRACT

UHRF1 (ubiquitin-like, containing PHD and RING finger domains, 1) recruits DNMT1 to hemimethylated DNA during replication and is essential for maintaining DNA methylation. *uhrf1* mutant zebrafish have global DNA hypomethylation and display embryonic defects, including a small liver, and they die as larvae. We make the surprising finding that, despite their reduced organ size, *uhrf1* mutants express high levels of genes controlling S-phase and have many more cells undergoing DNA replication, as measured by BrdU incorporation. In contrast to wild-type hepatocytes, which are continually dividing during hepatic outgrowth and thus dilute the BrdU label, *uhrf1* mutant hepatocytes retain BrdU throughout outgrowth, reflecting cell cycle arrest. Pulse-chase-pulse experiments with BrdU and EdU, and DNA content analysis indicate that *uhrf1* mutant cells undergo DNA re-replication and that apoptosis is the fate of many of the re-replicating and arrested hepatocytes. Importantly, the DNA re-replication phenotype and hepatic outgrowth failure are preceded by global loss of DNA methylation. Moreover, *uhrf1* mutants are phenocopied by mutation of *dnmt1*, and Dnmt1 knockdown in *uhrf1* mutants enhances their small liver phenotype. Together, these data indicate that unscheduled DNA replication and failed cell cycle progression leading to apoptosis are the mechanisms by which DNA hypomethylation prevents organ expansion in *uhrf1* mutants. We propose that cell cycle arrest leading to apoptosis is a strategy that restricts propagation of epigenetically damaged cells during embryogenesis.

KEY WORDS: DNA methylation, DNA replication, Hepatic outgrowth, Liver development, UHRF1, Zebrafish

INTRODUCTION

Epigenetics is a fundamental mechanism underlying gene regulation and chromatin structure. Despite the crucial role epigenetics plays throughout biology, how the fidelity of the epigenome is monitored and maintained during cell division is poorly understood. Ubiquitin-like, containing PHD and RING finger domains, 1 (UHRF1) reads epigenetic marks and enlists chromatin modifiers to propagate these marks to daughter cells. UHRF1 has a conserved function across vertebrates as an essential component of the DNA methylation machinery; it binds hemi-methylated DNA generated during DNA replication and recruits DNA methyltransferase 1 (DNMT1) to methylate cytosines on newly synthesized DNA (Arita et al., 2008; Avvakumov et al., 2008; Bostick et al., 2007; Hashimoto et al., 2008; Qian et al., 2008; Sharif et al., 2007). UHRF1 also promotes the activity, specificity and degradation of DNMT1 (Bashtrykov et al., 2014; Berkyurek et al., 2014; Qin et al., 2011). Thus, UHRF1 serves to both promote and restrict DNA methylation and, consequently, both loss (Bostick et al., 2007; Feng et al., 2010; Sharif et al., 2007) and overexpression (Mudbhary et al., 2014) of UHRF1 restructures the methylome.

Epigenetics contributes to the expression of most, if not all, genes. Therefore, it is assumed that the cellular phenotypes resulting from altering epigenetic modifiers are attributed to direct changes in the expression of genes that are under epigenetic control. For example, *Uhrf1*-deficient mouse T-cells have increased *Cdkna1* expression that is associated with reduced methylation in its promoter (Obata et al., 2014), and this epigenetic derepression could account for its upregulation. An alternative hypothesis is that a surveillance mechanism for epigenetic damage elicits a cellular response to prevent propagation of cells with epigenetic damage, analogous to the DNA damage response (Milutinovic et al., 2003). This epigenomic stress response then induces genes to prevent cell cycle progression, by a mechanism that is not a direct result of loss of epigenetic-mediated repression (Milutinovic et al., 2004), but instead to prevent passive loss of DNA methylation (Milutinovic et al., 2003; Unterberger et al., 2006). The mechanisms underlying the cellular response to UHRF1 loss or overexpression are not fully understood.

Most studies on UHRF1 in mammals have been carried out in cultured malignant cells, because mouse *Uhrf1* mutants die early in gestation (Bostick et al., 2007; Muto et al., 2002; Sharif et al., 2007), and tissue-specific knockout models have only recently been generated (Obata et al., 2014). UHRF1 depletion from cancer cells results in a variety of phenotypes, including cell cycle arrest (Li et al., 2011; Tien et al., 2011), apoptosis (Tien et al., 2011), loss of contact inhibition (Hopfner et al., 2002) and increased sensitivity to DNA-damaging agents (Arima et al., 2004; Mistry et al., 2010; Muto et al., 2002). Similar phenotypes have also been reported for DNMT1-deficient cells (Chen et al., 2007; Karpf and Matsui, 2005; Milutinovic et al., 2003; Unterberger et al., 2006; Vijayaraghavalu et al., 2013), suggesting DNA hypomethylation as the underlying cause of these phenotypes.

Zebrafish *uhrf1* mutants survive to later developmental stages than mouse embryos because maternal supplies support early development (Chu et al., 2012). Mutant embryos display defects in

[1]Department of Medicine, Division of Liver Diseases, Icahn School of Medicine at Mount Sinai, 1 Gustave L. Levy Place, Box 1020, New York, NY 10029, USA. [2]Department of Developmental and Regenerative Biology, Icahn School of Medicine at Mount Sinai, 1 Gustave L. Levy Place, Box 1020, New York, NY 10029, USA. [3]Graduate School of Biomedical Sciences, Icahn School of Medicine at Mount Sinai, 1 Gustave L. Levy Place, Box 1020, New York, NY 10029, USA. [4]Liver Cancer Program, Tisch Cancer Institute, Icahn School of Medicine at Mount Sinai, 1 Gustave L. Levy Place, Box 1020, New York, NY 10029, USA. [5]Division of Gastroenterology and Hepatology, University Medicine Cluster, National University Health System, Singapore.

*Author for correspondence (kirsten.edepli@mssm.edu)

Received 30 July 2014; Accepted 18 November 2014

Development (2015) 142, 510-521 doi:10.1242/dev.115980

multiple tissues, including the liver and eye (Sadler et al., 2007; Tittle et al., 2011). In wild-type (WT) larvae, a distinct liver bud is visible by 3 days post fertilization (dpf) and during the next 2 days, hepatocyte division and organ morphogenesis collaborate to form the bi-lobed crescent-shaped mature larval liver. In *uhrf1* mutants, the hepatic bud forms but does not expand so that 5 dpf *uhrf1* mutants have a small, unilobular, ball-shaped liver (Sadler et al., 2007). Apoptosis is likely one mechanism underlying the small organ size in *uhrf1* mutants, as both the liver (Sadler et al., 2007) and eye (Tittle et al., 2011) have more cell death than wild-type larvae. However, reduced proliferation, as found in Dnmt1-depleted cells in culture (Milutinovic et al., 2003; Unterberger et al., 2006) and Uhrf- deficient T-regulatory cells (Obata et al., 2014) may also contribute to the *uhrf1* mutant phenotype.

In this study, we sought to understand the epigenetic and cellular basis for the small liver phenotype of *uhrf1* mutant embryos. We made the surprising discovery that genes regulating DNA replication and S phase were significantly upregulated in whole *uhrf1* mutant larvae, and this was even more evident in mutant livers, despite their small size. There was a striking increase in the number of cells that incorporate bromodeoxyuridine (BrdU) as an indication of DNA replication; however, these cells did not progress in the cell cycle and ultimately died. Because (1) DNA methylation is the most robustly depleted epigenetic mark in *uhrf1* mutants, (2) *dnmt1* mutants phenocopy the cell cycle defects observed in *uhrf1* mutants and (3) loss of Dnmt1 enhances the hepatic phenotype of *uhrf1* mutants, we conclude that DNA hypomethylation is the mechanism underlying the cell cycle block and small liver phenotype caused by *uhrf1* depletion. We speculate that cell cycle arrest is a mechanism to limit propagation of cells with epigenetic damage during embryogenesis.

RESULTS

The *uhrf1* mutant phenotype is preceded by loss of uhrf1 mRNA

We sought to define time course of the *uhrf1* mutant phenotype. As reported previously (Tittle et al., 2011), all *uhrf1* mutants died by 240 h post fertilization (hpf), with a median survival of 192 hpf (Fig. 1A). We then asked how this correlated with the depletion of *uhrf1* mRNA. The $uhrf1^{hi272}$ allele used in this study is caused by a viral insertion in the first intron of the *uhrf1* gene [supplementary material Fig. S1A (Amsterdam et al., 2004)]. These insertions frequently cause nonsense-mediated decay of the resultant message (Amsterdam et al., 2004). Wild-type and mutant embryos were sorted based on morphological phenotype at 4 and 5 dpf, and younger mutants were individually genotyped. Pools of wild-type or mutant embryos were used for RNA extraction. Primers located on exons flanking the viral insertion for PCR detected low levels of accurately spliced message in mutant larvae, suggesting some transcripts from the mutant allele escape the RNA decay process (supplementary material Fig. S1B). Thus, the $uhrf1^{hi272}$ allele is a hypomorphic mutation. Primers downstream of the insertion used for quantitative real time PCR (qPCR; Fig. 1B; supplementary material Fig. S1C) detected a significant reduction of *uhrf1* transcripts to 25% of wild-type levels from 48 hpf onwards (Fig. 1B), indicating that maternal mRNA is present in *uhrf1* mutants through 24 hpf.

To determine the correlation between the appearance of morphological defects with the reduction of *uhrf1* message, we monitored the same embryos from 48 hpf to 120 hpf (Fig. 1C). *uhrf1* is most highly expressed in the jaw, head, eyes, liver and gut (Sadler et al., 2007), and these tissues are highly proliferative during the time points after *uhrf1* mRNA is depleted. Defects in these

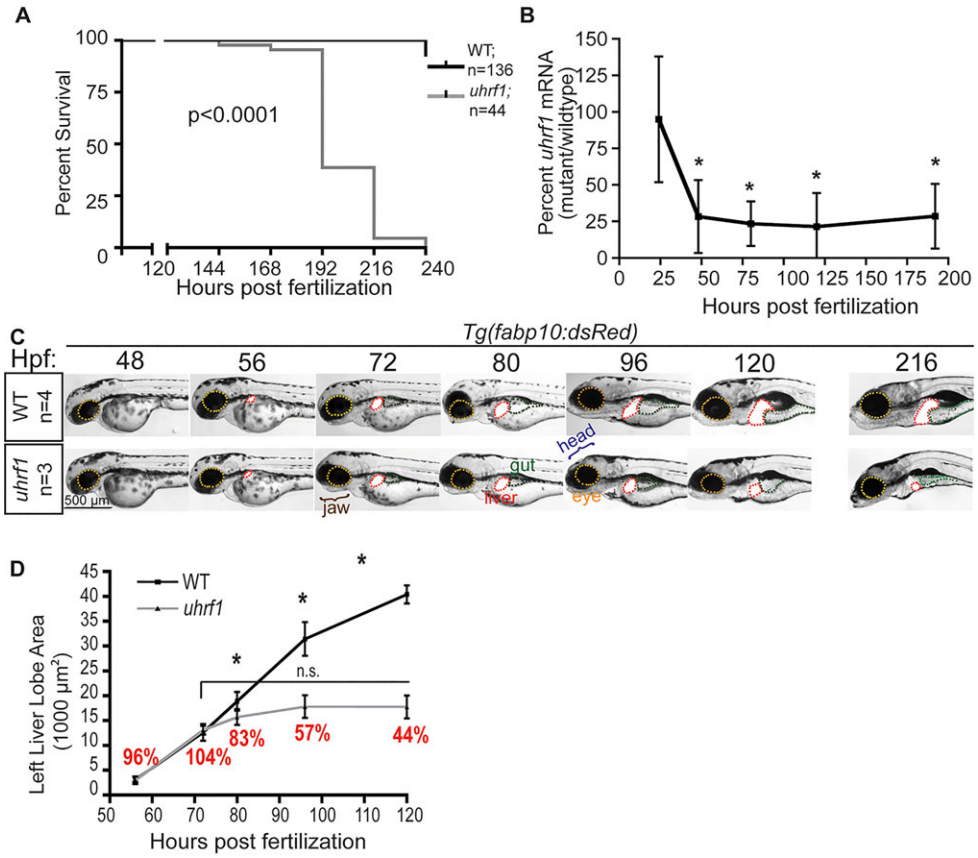

Fig. 1. Reduction in *uhrf1* mRNA expression precedes onset of mutant phenotype. (A) Cumulative survival of *uhrf1* mutant larva and wild-type siblings. (B) *uhrf1* mRNA levels were measured by qPCR over a period of 25-200 hours post fertilization (hpf). Embryos were individually genotyped prior to 72 h to identify mutants and older larvae were sorted based on morphological phenotype. Data are average fold change in expression from three or more clutches. **P*<0.05 by Student's *t*-test. (C) The same wild-type and *uhrf1* mutant embryo was imaged every day, except at 216 hpf, when larvae from a separate clutch were used. Labels on the head, jaw, eye, liver (highlighted using the *fabp10:dsRed* transgene) and gut indicate the first time point at which defects in these tissues become visible in *uhrf1* mutants. (D) Left liver lobe area was measured in four wild-type and three mutant larvae at 56-120 hpf. The relative size of the *uhrf1* mutant liver relative to wild-type siblings is labeled in red. **P*<0.05 by Student's *t*-test, error bars are s.d.

Development (2015) 142, 510-521 doi:10.1242/dev.115980

structures were first detected between 72 and 80 hpf, and become exacerbated at the larval stage (Fig. 1C).

Tg(fabp10:dsRed) fish that express dsRed in hepatocytes (Dong et al., 2007) were used to focus on the effects of *uhrf1* mutation on the liver. Transgene expression in the hepatic bud is first visible in both wild-type and mutant larvae by 56 hpf (Fig. 1C). Expansion of the hepatic bud begins at 3 dpf in wild-type larvae, so that size of the left liver lobe nearly triples by 5 dpf (Fig. 1C,D). The liver appears normal in *uhrf1* mutants until 72 hpf but it does not expand afterwards (Fig. 1D), indicating failed hepatic outgrowth.

Genes promoting S-phase and DNA replication are upregulated in *uhrf1* mutants

We analyzed gene expression using microarray analysis of two samples of mRNA pooled from 120 hpf wild-type and mutant larvae as the phenotypes are clearly apparent in all organs at this time. This identified 248 genes as significantly differentially expressed in *uhrf1* mutants (117 upregulated, 131 downregulated; supplementary material Table S1). Gene Set Enrichment Analysis (GSEA; supplementary material Table S2) on all differentially expressed genes revealed many involved in the cell cycle and S phase, which made up the largest fraction (41%) of upregulated pathways identified in the Reactome Database (www.reactome.org) (Fig. 2A; supplementary material Fig. S2, Tables S2 and S3). Sixty-three of the 86 genes in the S-phase gene set identified as deregulated in *uhrf1* mutants were upregulated, including S-phase cyclins, and DNA replication licensing and processivity factors (Fig. 2B; supplementary material Table S3). qPCR analysis of a subset of these confirmed all were upregulated in whole-mutant larvae by 120 hpf. Some (*mcm2*, *mcm4*, *cdc6*, *orc6*, *pold2*; $P<0.05$) were induced by ~2 fold as early as 80 hpf, but none was upregulated at earlier time points (Fig. 2C). Mcm3, a component of the pre-replication complex, and Pcna, a key processivity factor, were also upregulated at the protein level in 120 hpf whole *uhrf1* mutant larvae (Fig. 2D). There was a greater upregulation of all genes in mutant livers at 120 hpf, and two genes (*ccnd1*, *pola1*) were modestly (~1.6 fold), but significantly, induced in the liver as early as 80 hpf ($P<0.05$; Fig. 2E).

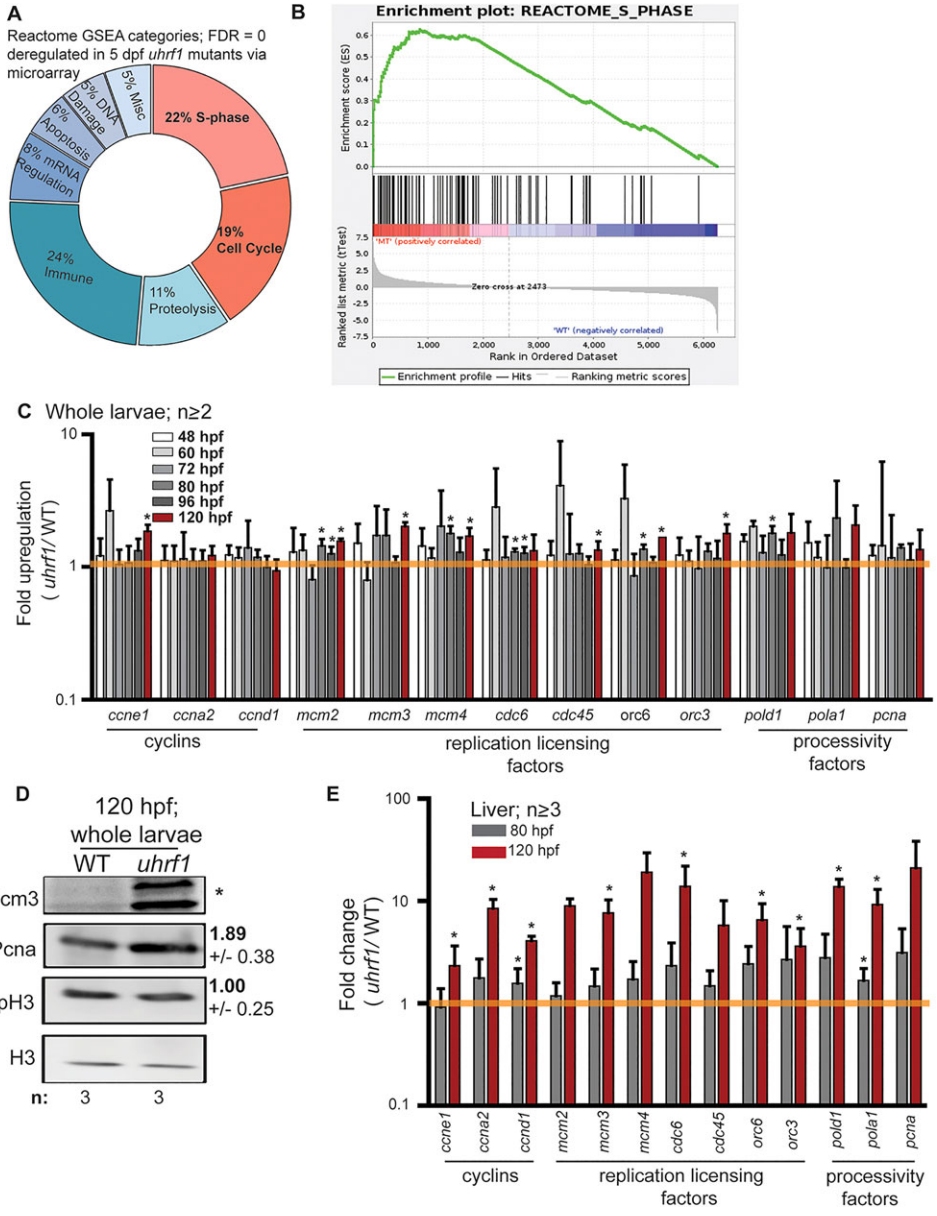

Fig. 2. DNA replication and S-phase genes are upregulated in *uhrf1* mutants. (A) GSEA categories as defined by the curated molecular pathway in the Reactome database. (B) Enrichment plot of S-phase genes. (C) A subset of genes identified in A and B was analyzed by qPCR from whole larva that were individually genotyped at 48-72 hpf or separated based on phenotype (80-120 hpf); embryos from two or more clutches were pooled for each time point and the average fold change in *uhrf1* mutants is graphed. (D) Western blot of pooled whole larvae at 120 hpf. The average fold change of the ratio to H3 from three samples are indicated with the s.d. and *$P<0.05$ by Student's *t*-test. There was no Mcm3 detected in the wild-type samples, precluding calculation of fold change. (E). qPCR was used to measure gene expression in dissected liver samples. Student's *t*-test on $\Delta\Delta$Ct values (C,E) or protein levels normalized to H3 (D) was used to determine significance.*$P<0.05$. Error bars represent s.d.

Development (2015) 142, 510-521 doi:10.1242/dev.115980

As *uhrf1* mutants are characterized by reduced organ size, we were surprised that genes typically associated with cell proliferation were upregulated. We reasoned that this could either reflect the epigenetic de-repression of these genes uncoupled from DNA replication, or could reflect an increased number of cells in S phase. DNA methylation of CpG islands in gene promoters is frequently inversely correlated with gene expression. Not all of the S-phase regulatory genes that are upregulated in *uhrf1* mutants have CpG islands within 10 kb of their transcription start site (TSS; supplementary material Table S4), although this does not categorically rule out the possibility that they are regulated by DNA methylation. We mined previously generated genome-wide shotgun bisulfite sequencing data from 120 hpf wild-type and *uhrf1* mutants (Feng et al., 2010), and did not find significant differences in the level of methylation in the presumed regulatory regions for most of these genes (supplementary material Table S5). Importantly, the low depth read from this analysis did not allow comparison of the same residues in both samples and deeper sequencing is required to fully examine whether the methylation status of these genes could contribute to their deregulation in *uhrf1* mutants.

We next assessed BrdU incorporation to determine whether the gene expression differences reflected functional differences in DNA replication. Wild-type larvae exposed to BrdU from 120 to 124 hpf have high incorporation in rapidly expanding tissues (jaw, fin, eye) and lower incorporation in organs nearing the end of their proliferative phase (liver, muscle; Fig. 3B). By contrast, cells throughout *uhrf1* mutant larvae incorporated BrdU with over 3 times the number of BrdU-positive hepatocytes (49% versus 15%; Fig. 3B). Together with the gene expression analysis, these data indicate that *uhrf1* mutation increases the number of cells in S-phase and this is most profound in highly proliferating tissues, such as the liver. A previous report found reduced proliferation markers in the eye of 4 dpf *uhrf1* mutants (Tittle et al., 2011), but using our prolonged BrdU exposure protocol on 5 dpf we detected no difference in BrdU incorporation between wild-type and mutant cells in the eye (43/135 wild-type cells; 32% versus 54/159; 34% *uhrf1* mutant cells). This may reflect tissue-specific differences in the response to Uhrf1 depletion.

uhrf1 mutant cells undergo cell cycle arrest

Our findings suggest either that *uhrf1* mutant hepatocytes are hyperproliferative, which is inconsistent with the small liver phenotype, or that they are undergoing DNA replication but fail to divide. To distinguish between these possibilities, we carried out the pulse-chase experiment outlined in Fig. 3A: wild-type and *uhrf1* mutant larvae were incubated with BrdU at 5 dpf for 4 h, after which the BrdU was washed out and larvae were collected 7, 26 and 42 h after the BrdU pulse. At each time point, livers were dissected from three to five larvae from each genotype and processed for immunofluorescence; histone H3 staining marked all nuclei and BrdU marked cells that were in S phase during the 4 h pulse. As expected, the percent of BrdU-positive cells in wild-type larvae increased after 7 h as the label was passed to daughter cells (Fig. 3C; supplementary material Fig. S3A) and as cells continued to divide, BrdU was diluted and thus the positive fraction decreased to less than 20% by 42 h (Fig. 3C; supplementary material Fig. S3). By contrast, 50% or more of *uhrf1* mutant cells were BrdU positive at all time points (Fig. 3C; supplementary material Fig. S3). Wild-type cells therefore display a dynamic change in BrdU label over time that reflects their proliferation, whereas mutant cells display a static retention of BrdU label, indicating they are either arrested or cycle very slowly.

DNA damage and replication stress cause cells to halt DNA synthesis and arrest in S phase. To determine whether the same *uhrf1* mutant cells that incorporated BrdU but did not cycle were continually undergoing DNA synthesis, we pulsed larvae with BrdU at 72 hpf then removed it. At 120 h, larvae were pulsed with a different nucleotide, EdU, and processed for immunodetection of both labels. We found that 2/96 (2%) of wild-type but 9/92 (10%) of *uhrf1* mutant hepatocytes were positive for both nucleotides (Fig. 3D). This indicates that these dual-labeled cells underwent DNA replication at 3 dpf and continued to replicate 2 days later. We also found that *uhrf1* mutant hepatocyte nuclei contained more DNA-based on Sytox Green staining (Fig. 3E) and were almost twice as large as wild-type nuclei (supplementary material Fig. S4A,B); while hepatocyte size was also larger in mutants (supplementary material Fig. S4A,B), the nucleus was disproportionately larger (supplementary material Fig. S4C) (Fig. 3E). Together, these data suggest that *uhrf1* mutant hepatocytes undergo DNA re-replication coupled with a cell cycle block that prevents their division.

Cell cycle arrest results in apoptosis

Cell cycle checkpoints restrain the cell for a limited time, and cells that bypass checkpoints frequently undergo apoptosis. *uhrf1* mutant zebrafish are characterized by widespread apoptosis (Sadler et al., 2007; Tittle et al., 2011) and we performed the experiment outlined in Fig. 3F to ask whether the hepatocytes that incorporate BrdU contribute to the population of dying cells. Larvae pulsed with BrdU for 1 h at the onset of hepatic outgrowth (72 hpf) were chased until the end of hepatic outgrowth (120 hpf) and the livers were assessed for both BrdU incorporation (Fig. 3F) and TUNEL staining (Fig. 3G). Wild-type cells lost the BrdU label during the 47 h chase, whereas the mutant liver was full of BrdU cells, demonstrating cell cycle arrest of mutant hepatocytes (Fig. 3G). Although there were no TUNEL-positive cells in wild-type livers, up to 5% of BrdU-positive cells were also TUNEL positive, indicating that apoptosis is one fate of *uhrf1* mutant cells that fail to divide.

Cell cycle arrest is an acute response to *uhrf1* loss

If cell cycle arrest leading to apoptosis is the primary cellular defect caused by Uhrf1 loss, then cell death should occur just after *uhrf1* mRNA is depleted (48 hpf) and prior to gross morphological phenotypes (80 hpf). We found that mutant embryos have increased Acridine Orange labeling as an indication of dead cells in the jaw and head at 72 hpf (Fig. 4A), prior to the profound morphological defects that occur in these structures at later time points (Fig. 1C). We asked whether the cell cycle arrest of *uhrf1* mutant cells occurred prior to this cell death phenotype through the experiment outlined in Fig. 4B. Embryos were pulsed with BrdU for 1 h at 56 hpf and assessed at 72 hpf. This analysis revealed few BrdU-positive cells in wild-type embryos following the 15 h chase, but cells throughout mutant embryos retained the label (Fig. 4B), demonstrating that wild-type cells proliferated between 56 and 72 hpf, whereas mutant cells did not. Importantly, this BrdU retention phenotype is established at 56 hpf, prior to widespread cell death starting at 72 hpf, suggesting that cell cycle arrest is the primary cellular response to *uhrf1* loss in primary cells.

To determine whether this acute cell cycle block in *uhrf1* mutants contributed to the *uhrf1* mutant phenotype at 120 hpf, we used a heat-shock inducible transgene [*Tg(hsp70l:UHRF1-GFP)* (Chu et al., 2012)] to replace UHRF1 expression transiently in the embryo at 24, 32, 54 and 72 hpf, and then assessed larvae at 120 hpf for overall (Fig. 4C) and hepatic (Fig. 4D) defects. Heat-shock inducing

Development (2015) 142, 510-521 doi:10.1242/dev.115980

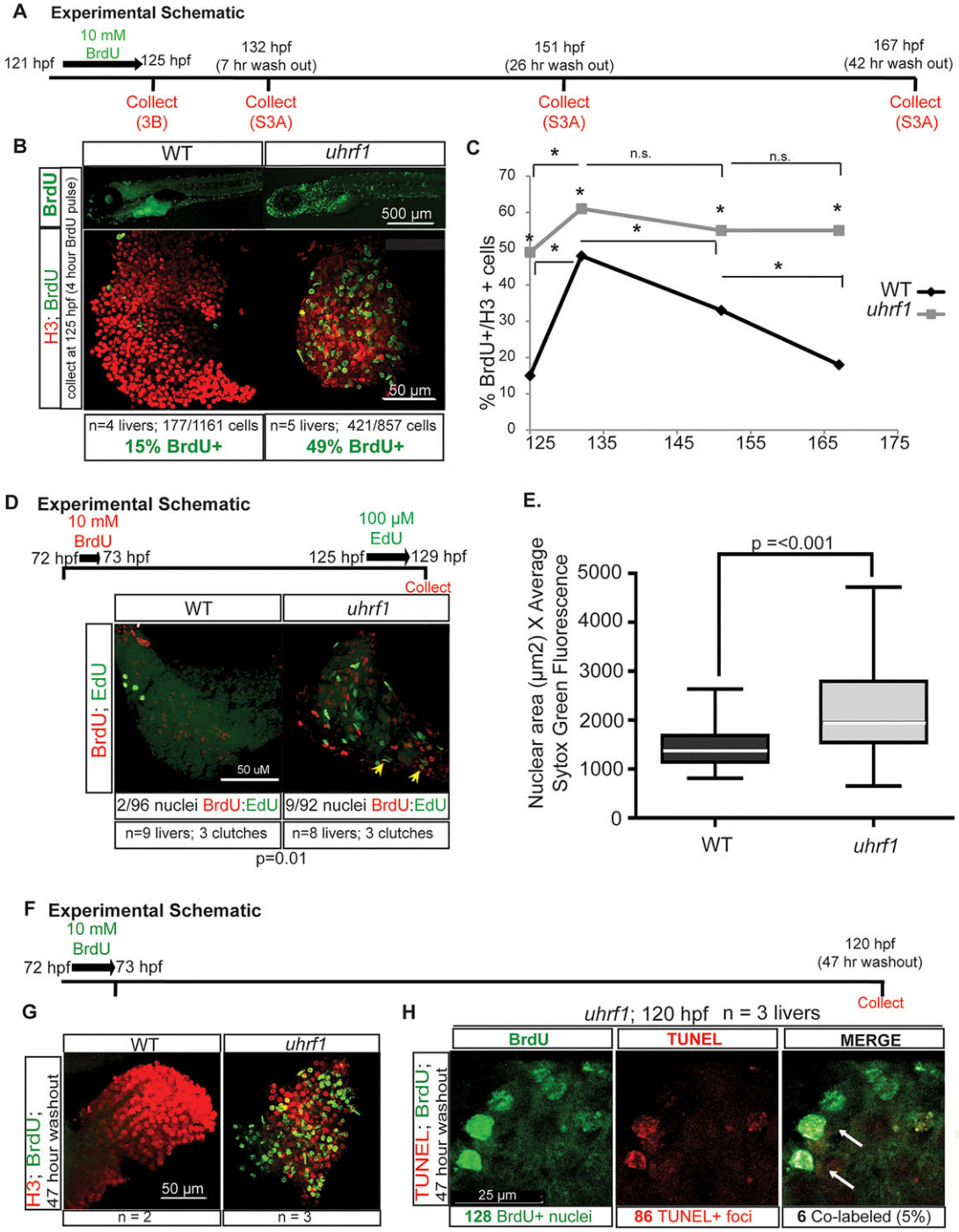

Fig. 3. *uhrf1* mutant hepatocytes apoptose after failing to proceed through S phase. (A) BrdU pulse-chase experiment overview. The figures and figure panels containing the data from each collection point are indicated. (B) Immunofluorescence for BrdU and H3 to label all nuclei on livers from *uhrf1* and wild-type larvae collected at 124 hpf, immediately after BrdU pulse. BrdU- and H3-positive cells were counted for four or five livers per genotype. (C) Average number of BrdU-positive nuclei in three to five livers per sample relative to nuclear H3 (see panel B and supplementary material Fig. S3D for raw numbers). Asterisks on the gray line indicate $P<0.05$ when comparing mutant and wild-type values; asterisks or n.s. (not significant) above the bars indicate differences between samples of the same genotype at different times. (D) Schematic of BrdU pulse at 72 hpf chased with EdU at 125 hpf. Livers were processed for both nucleotide analogs to determine percent of co-labeled nuclei. (E) Relative DNA content in *uhrf1* compared with wild-type hepatocytes at 125 hpf, as measured by Sytox Green staining. Top and bottom of box plot designate 75% and 25% of the population, respectively, separated by the median; bars represent 10th and 90th percentiles. (F) BrdU pulse-chase experiment outline. (G) Embryos treated for 1 h with 10 mM BrdU at 72 hpf were collected at 120 hpf (47 h post-washout) and stained for H3 and BrdU. (H) Hepatocyte nuclei with both BrdU and TUNEL staining are labeled with white arrows.

transient expression of UHRF1-GFP (supplementary material Fig. S4A,B) had no effect on wild-type larvae, but heat shock at 32 and 54 hpf significantly reduced the gross morphological defects (Fig. 4C) and increased liver size in *uhrf1* mutants from 41% of wild-type liver size in non-heat shocked mutants to 67 and 71% of controls, respectively (Fig. 4C,D). Interestingly, the UHRF1 produced from the heat shock at 32 hpf is barely detectable by 72 hpf, similar to the duration of the protein produced from heat

Development (2015) 142, 510-521 doi:10.1242/dev.115980

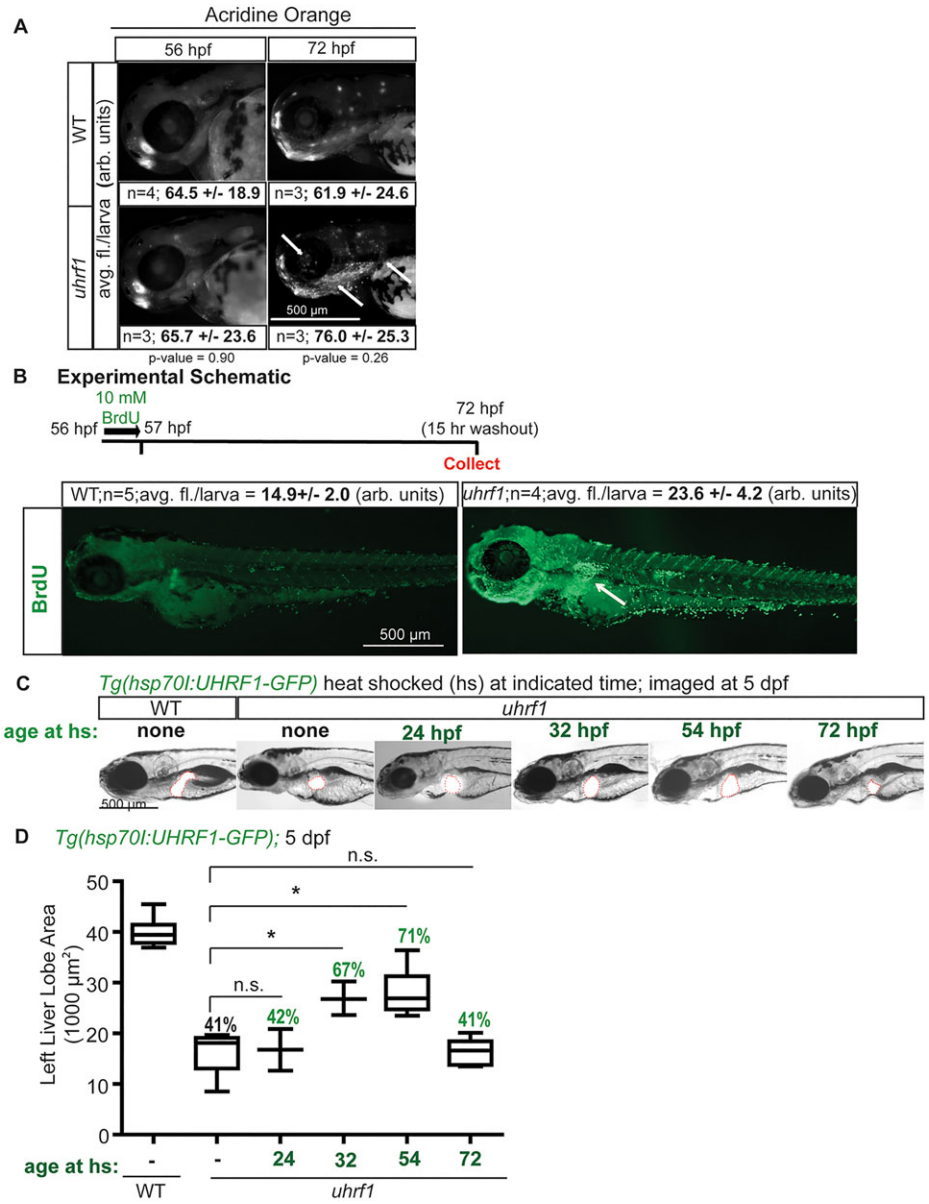

Fig. 4. Cell cycle arrest is an acute response to the loss of *uhrf1*. (A) Acridine Orange staining of whole fish was imaged at 56 and 72 hpf. Averaged intensity of fluorescence from the head, jaw and ear of three or four larvae (*n*) is indicated with the s.d. Arrows point to the regions with enhanced cell death in mutant larvae. (B) Whole fish were pulsed with BrdU at 56 hpf for 1 h and processed for BrdU immunofluorescence at 72 hpf. Arrow points to intense labeling in the liver. (C) *Tg(hsp70l:UHRF1-GFP; fabp10:ds-Red);uhrf1* and wild-type siblings were heat-shocked to induce expression of UHRF1 at the indicated times. The liver is outlined in red. (D) The left liver lobe area was quantified in three or four fish per time point. All fish contain the *Tg(hsp70l:UHRF1-GFP)* transgene. Heat shock had no effect on liver size in WT fish. Box plots are as described in Fig. 3E. **P*<0.05 by Student's *t*-test. The percent difference in the area of the left liver lobe of the mutants relative to wild-type is indicated.

shock at 72 hpf (supplementary material Fig. S5A,B). A single heat shock at 48 hpf could partially prevent DNA hypomethylation in 5 dpf *uhrf1* mutants (supplementary material Fig. S5C). Heat shock at 72 hpf does not rescue liver size because, by this time, the mutant phenotype is already well under way (Fig. 1C, Fig. 4A,B). This supports our hypothesis that cell cycle arrest caused by Uhrf1 loss restricts organ size.

Uhrf1 functions in a cell-autonomous fashion to regulate hepatic outgrowth

We next asked whether Uhrf1 was required in a cell-autonomous fashion during hepatic outgrowth by crossing *uhrf1* mutants to a transgenic line expressing low levels of UHRF1-GFP exclusively in hepatocytes [*Tg(fabp10:UHRF1-GFP)*^{LOW}, hereafter referred to as *UHRF1-GFP Low*] (Chu et al., 2012; Mudbhary et al., 2014). The non-hepatic phenotypes were not altered in *uhrf1* mutants expressing *UHRF1-GFP Low* in hepatocytes (Fig. 5A), but liver size was partially restored (Fig. 5B). Although *UHRF1-GFP Low* expression in wild-type livers had no effect on liver size (Fig. 5A,B) (Mudbhary et al., 2014) or on the expression of the cell cycle gene panel we examined (not shown), there was a significant effect on most genes in *uhrf1* mutants. For example, *ccna2* expression in *uhrf1* mutant livers expressing UHRF1-GFP was induced to only 44% of the level detected in *uhrf1* mutants lacking UHRF1-GFP (*P*<0.05; Fig. 5C). Moreover, TUNEL labeling was reduced (Fig. 5D), survival was significantly improved (Fig. 5E) and DNA hypomethylation was partially prevented (see Fig. 6C). We thus conclude that Uhrf1 functions in a cell-autonomous fashion in hepatocytes to promote cell cycle progression and hepatic outgrowth, and that the mortality of *uhrf1* mutants is, in part, attributed to failed hepatic outgrowth.

DNA methylation is the only epigenetic mark depleted in *uhrf1* mutants

Loss of Uhrf1 causes global DNA hypomethylation in human, mouse and zebrafish cells (Bostick et al., 2007; Feng et al., 2010; Hervouet et al., 2010; Sharif et al., 2007; Tittle et al., 2011). In addition, UHRF1 has been implicated in histone deacetylation (Achour et al., 2009; Papait et al., 2008; Unoki et al., 2004) and histone H3 trimethylation [H3K9me3 (Cheng et al., 2013; Kim et al., 2009; Rottach et al., 2010;

Development (2015) 142, 510-521 doi:10.1242/dev.115980

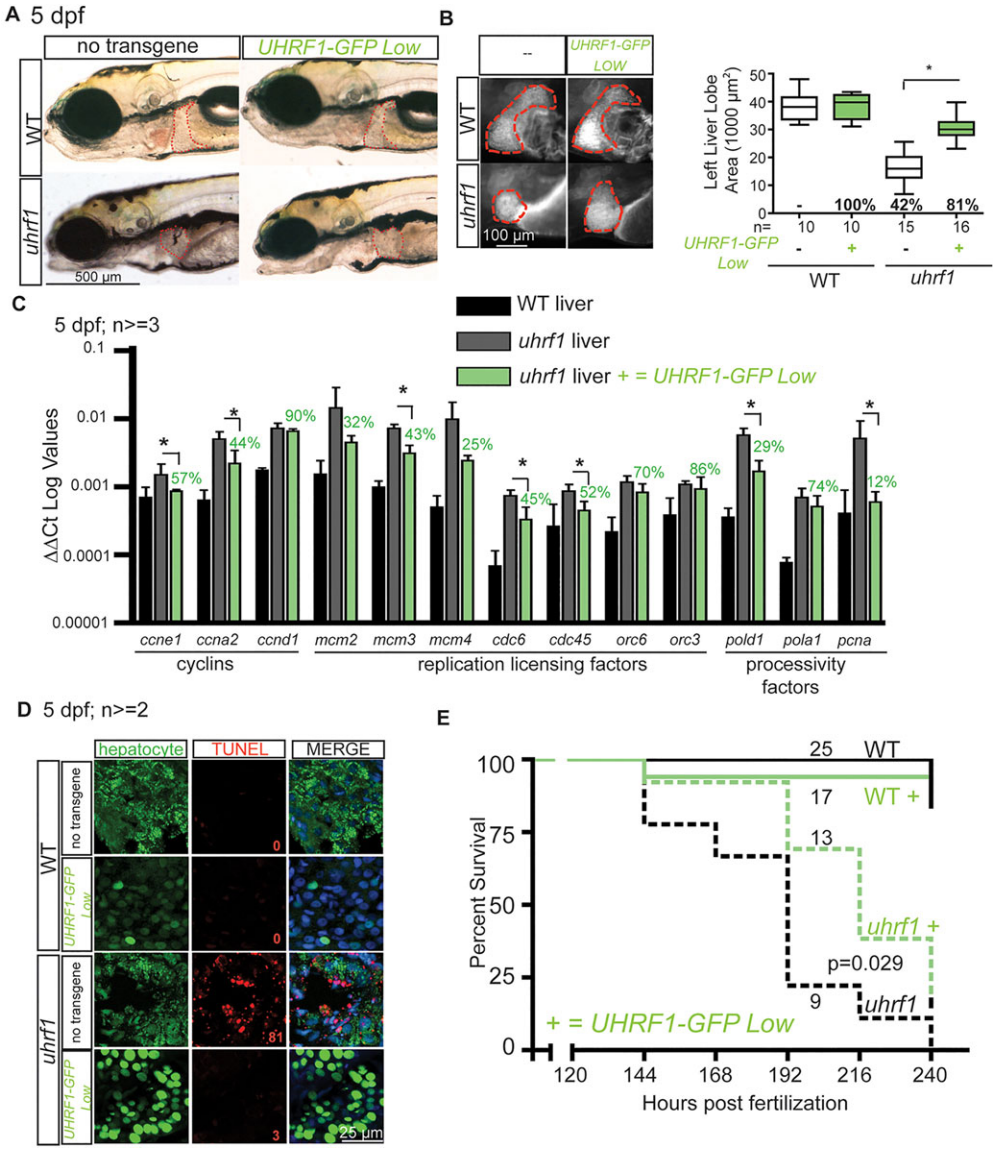

Fig. 5. Uhrf1 acts cell-autonomously to regulate liver outgrowth. (A) Wild-type and *uhrf1* 5 dpf larvae with or without the *Tg(fabp10:UHRF1-EGFP) Low* transgene. The liver is outlined. (B) The area of the left liver lobe was quantified in 10-16 larvae from three clutches of each genotype (left panel). Top and bottom of box plot designate 75% and 25% of the population, respectively, separated by the median; bars represent 10th and 90th percentiles. **P*<0.05. The percent relative to wild-type liver is indicated. (C) qPCR on cDNA from dissected livers. Student's *t*-test was used to determine significance between ΔΔCt values of *uhrf1* mutants with and without the *Tg(fabp10:UHRF1-EGFP)Low* transgene and percentage of upregulation in mutants with and without the transgene is indicated. (D) Representative image of more than two TUNEL-stained livers from each sample with the average number of TUNEL (+) foci for each sample indicated in red. Livers without the UHRF1-EGFP expression were stained with Cy5-SA to highlight hepatocytes. (E) Cumulative survival of one cohort of fish. The number of animals in each sample is indicated. Log rank test was used to calculate *P*-value.

Xie et al., 2012)] at specific loci in mammalian cells. We assessed global levels of histone acetylation and H3K9me3 by western blotting (Fig. 6A) and of DNA methylation by slot blotting for 5-MeC (Fig. 6B) in *uhrf1* mutants and their wild-type siblings. Only DNA methylation was significantly reduced in *uhrf1* mutants, and it was comparable with levels detected in *dnmt1* mutant larvae (Tittle et al., 2011) (Fig. 7A). DNA hypomethylation was detected as early as 48 hpf in *uhrf1* mutants (Fig. 6B) and persisted through 5 dpf (Fig. 6B). Immunostaining for 5-MeC revealed a reduction in *uhrf1* mutant muscle at 72 and 120 hpf (supplementary material Fig. S6A), and a dramatic reduction in methylation in hepatocytes was found at 120 hpf (Fig. 6C; supplementary material Fig. S6B). DNA methylation was partially restored at 120 hpf by expression of UHRF1-GFP in hepatocytes (Fig. 6C). Moreover, all hepatocytes with BrdU incorporation in *uhrf1* mutants fail to stain with anti-5-MeC (supplementary material Fig. S7), demonstrating that DNA re-replication occurs in cells with DNA hypomethylation.

Despite this loss of DNA methylation, we found Dnmt1 protein to be increased at 5 dpf in *uhrf1* mutants by western blot of whole fish (Fig. 6D) and in 4 dpf hepatocytes by immunofluorescence (Fig. 6E), whereas *dnmt1* mRNA levels were not significantly higher (supplementary material Fig. S6C). This is consistent with a role for Uhrf1 in targeting Dnmt1 for degradation (Du et al., 2010; Mudbhary et al., 2014; Qin et al., 2011). We reasoned that the *uhrf1* mutant phenotype could be attributed to high Dnmt1 levels as Dnmt1 overexpression is embryonic lethal in mice (Biniszkiewicz et al., 2002). Alternatively, high levels of Dnmt1 in these *uhrf1* hypomorphic mutants may interact with the residual levels of Uhrf1 to facilitate some DNA methylation that might suppress a more severe phenotype. We assessed whether loss of Dnmt1 suppressed or enhanced the *uhrf1* mutant phenotype by identifying a concentration of *dnmt1* morpholino that reduced Dnmt1 protein (supplementary material Fig. S6E) and DNA methylation at 24 hpf (supplementary material Fig. S6F). Importantly, the overall phenotype (Fig. 6F) and small liver (Fig. 6G) in *uhrf1* mutants was enhanced by Dnmt1 knockdown, suggesting that DNA hypomethylation causes these phenotypes.

The S-phase arrest in *uhrf1* mutants is phenocopied by *dnmt1* mutation

dnmt1 mutants resemble *uhrf1* mutants in that they also fail to undergo hepatic outgrowth (Anderson et al., 2009), and they have

Development (2015) 142, 510-521 doi:10.1242/dev.115980

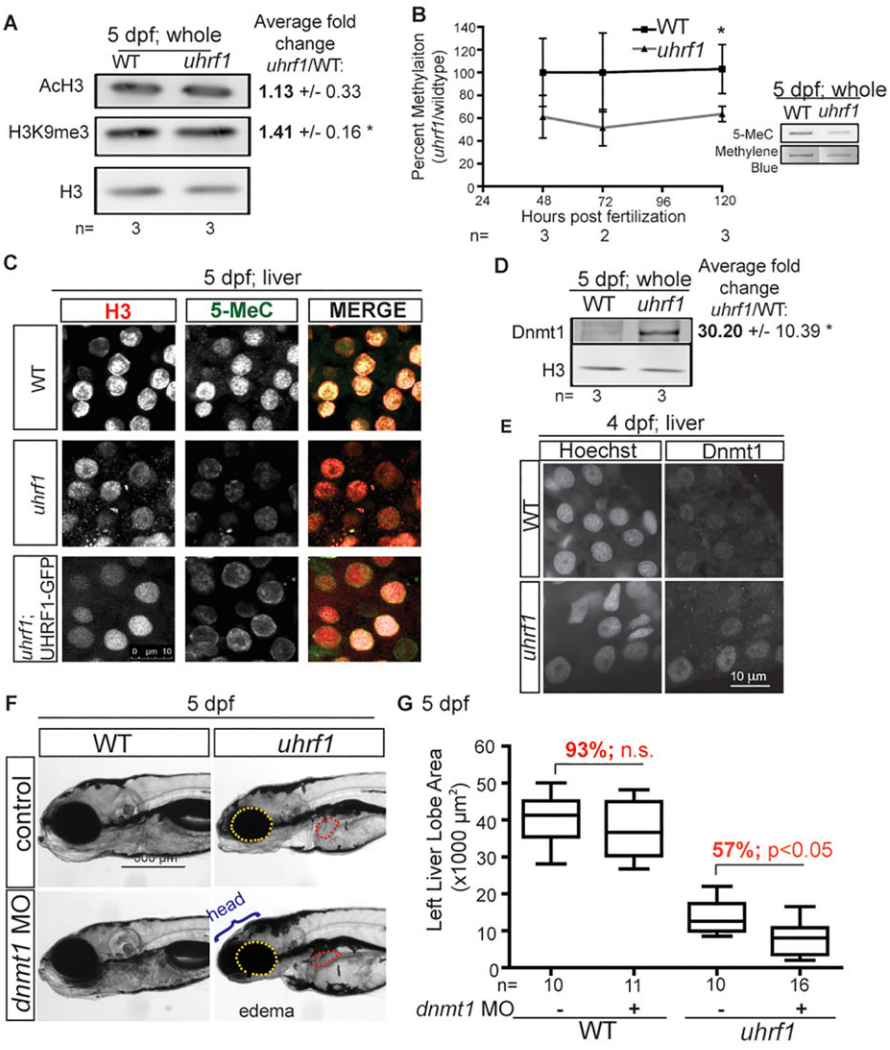

Fig. 6. The *uhrf1* mutant phenotype is mediated by hypomethylation. (A) Western blot of AcH3 and H3K9me3 levels in whole 5 dpf larvae normalized to H3. Average ratios to H3 from three clutches are indicated with the s.d. *P<0.05 by Student's t-test. (B) 5-MeC levels in *uhrf1* mutant embryos and wild-type siblings, as measured by slot blot from at least three clutches. Mutant embryos were identified by genotyping at 48-72 hpf and sorted based on morphological criteria at 96-120 hpf. (C) 5-MeC immunofluorescence on livers of 5 dpf wild type, *uhrf1* mutants and *Tg(fabp10:UHRF1-EGFP)Low*; *uhrf1* mutants. (D) Western blot of Dnmt1 in whole embryos. Average ratio of Dnmt1 to H3 in three clutches is indicated with the s.d. *P<0.05 by Student's t-test. (E) Dnmt1 immunofluorescence and Hoechst staining for DNA in livers of 4 dpf larvae. (F) Enhancement of the phenotypes in *uhrf1* mutants injected with *dnmt1* morpholino are indicated. (G) Quantification of left liver lobe size in 10-17 larvae on 5 dpf. Top and bottom of box plot designate 75% and 25% of the population, respectively, separated by the median; bars represent 10th and 90th percentiles. *P<0.05. The percentage of the average liver size in *dnmt1* morphants compared with the control injected larvae is indicated in red. n.s., not significant.

similar severe defects in the lens (Tittle et al., 2011). As previously reported (Tittle et al., 2011), the level of DNA methylation in 5 dpf *dnmt1* and *uhrf1* mutants was equivalent (Fig. 7A), despite the slight increase in *uhrf1* expression (supplementary material Fig. S5F). Importantly, *dnmt1* mutation also caused upregulation of cell cycle genes (Fig. 7B), Mcm3 and Pcna protein (Fig. 7C) and increased BrdU incorporation in hepatocytes at nearly identical levels to those detected in *uhrf1* mutants (Fig. 7D). As the S-phase arrest and hepatic outgrowth failure in *uhrf1* mutants is phenocopied by loss of Dnmt1, we conclude that DNA hypomethylation causes DNA re-replication coupled with a block in cell proliferation as a mechanism to prevent expansion of epigenetically damaged cells during embryogenesis.

DISCUSSION

Epigenetics is a central mechanism for regulating gene expression, and accurate epigenomic inheritance is essential for embryonic development. However, it is not clear whether the developmental defects that result from changes in the epigenome are attributed to aberrant gene expression or to a cellular response that prevents propagation of cells with epigenetic damage. Our data support this second model, as we find that both *uhrf1* and *dnmt1* mutation in zebrafish embryos induces unique cell cycle phenotype with enhanced expression of DNA synthesis machinery, ongoing DNA synthesis and a proliferation block culminating in apoptosis. We conclude that both a proliferative block and cell death lead to the small liver phenotype, and propose that this is a primary mechanism by which DNA hypomethylation restricts organogenesis. Whether a loss of epigenetic control of the expression of key cell cycle regulators also contributes to this phenotype, as has been observed in other systems (Obata et al., 2014), remains to be established.

By analyzing the developmental cascade initiated by *uhrf1* mutation, we establish a temporal sequence of molecular, cellular and developmental events that generate their small organ size phenotype (Fig. 8A). Maternal *uhrf1* mRNA is reduced by 48 hpf, resulting in DNA hypomethylation that is likely due to a passive mechanism, although a role for active DNA demethylation cannot be ruled out. Next, cell cycle arrest in S phase occurs between 56 and 72 hpf, and these arrested cells ultimately die; these two cellular responses prevent hepatic outgrowth and expansion in other tissues that undergo growth at later developmental stages. Failure of hepatic outgrowth, in part, leads to larval death.

Several lines of evidence support the conclusion that DNA hypomethylation is the cause of cell cycle arrest in *uhrf1* mutants: (1) zebrafish *dnmt1* mutants phenocopy the defects in the liver (Anderson et al., 2009; Sadler et al., 2007) and lens (Tittle et al., 2011);

Development (2015) 142, 510-521 doi:10.1242/dev.115980

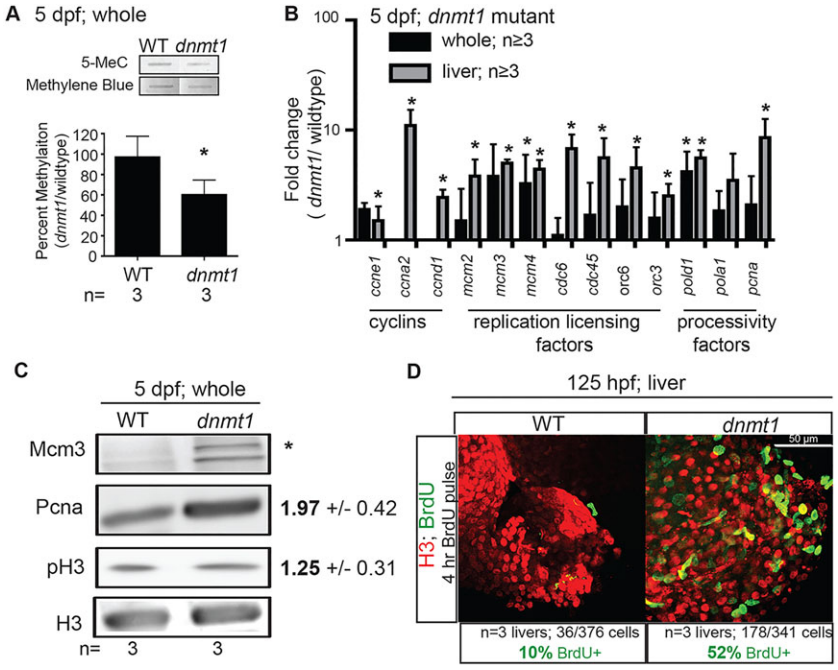

Fig. 7. The cell cycle phenotype in *uhrf1* mutants is phenocopied by *dnmt1* mutation. (A) Average levels of 5-MeC in 5 dpf whole *dnmt1* embryos and wild-type siblings was measured by slot blot in pools of embryos from three clutches. (B) qPCR of cell cycle genes from 5 dpf whole larvae (black) and dissected livers (gray) from three to five clutches of *dnmt1* mutants and wild-type siblings. Student's *t*-test on ΔΔCt values was used to determine significance; **P*<0.05. (C) Western blot of Mcm3, pH3 and PCNA in 5 dpf whole *dnmt1* wild-type and mutant fish with the average fold change of the ratio to H3 indicated for three samples ±s.d. There was no Mcm3 detected in wild-type larvae, precluding calculation of the fold change. (D) Representative image of BrdU and H3 immunoflourescence on a liver from *dnmt1* and wild-type larvae exposed to BrdU from 120 to 125 hpf. The average ratio of BrdU/H3-positive nuclei is indicated.

(2) hepatic outgrowth failure resembles zebrafish exposed to the Dnmt1 inhibitor 5-azacytidine (Mudbhary and Sadler, 2011); and (3) reducing Dnmt1 enhances the small liver size in *uhrf1* mutants (Fig. 6G). Although this finding does not preclude the possibility that another function of these two proteins contributes to the phenotype, the most straightforward conclusion is that the *uhrf1* cell cycle and small liver phentoype is caused by loss of DNA methylation. It is interesting that both *uhrf1* loss and overexpression in zebrafish hepatocytes cause DNA hypomethylation (Mudbhary et al., 2014), but the responses are quite distinct: *uhrf1* loss causes increased BrdU incorporation and apoptosis, whereas *uhrf1* overexpression causes cell cycle withdrawal and senescence (Mudbhary et al., 2014). Uhrf1 has been implicated in histone modifications, and it is possible that these different responses to epigenetic damage are mediated by other epigenetic changes that differ according to Uhrf1 levels.

The surprising finding from our study is that *uhrf1* mutation both increases DNA replication and blocks cell cycle progression (Fig. 8B). In contrast to the response to DNA damage or replication stress, where DNA replication is blocked, our data (that more cells have BrdU incorporation and genes that control S phase are induced in *uhrf1* and *dnmt1* mutants) suggest an increase in DNA replication. This is not reflective of a more actively dividing cell population, as the cells that incorporate BrdU at 72 hpf either cycle very slowly or not at all over the next 2 days. Thus, *uhrf1* mutant cells enter S phase and replicate their DNA, but either they do not exit S phase and continue to replicate or they divide very slowly. There is close coordination between DNA methylation, chromatin structure, DNA synthesis and replication timing. DNA replication origins fire first from euchromatin, and heterochromatin protects against re-firing (Dorn and Cook, 2011), as shown in *Arabidopsis thaliana*, where the maintenance of heterochromatin protects against re-replication (Jacob et al., 2010; Stroud et al., 2012) and possibly even endoreplication (Jegu et al., 2013). Thus, loss of Uhrf1 may alleviate a block to DNA re-replication, causing uncoordinated replication.

How does DNA hypomethylation block cell cycle progression? One possibility is that re-replication or DNA hypomethylation itself could induce DNA damage or genomic instability (Truong and Wu, 2011), activating a checkpoint. A previous study demonstrated that loss of UHRF1 in colon cancer cells causes a cell cycle arrest by activating a DNA damage checkpoint (Tien et al., 2011), whereas in other cell types, Uhrf1 loss causes a G1/S arrest (Arima et al., 2004), reminiscent of the checkpoint response occurring as a consequence of DNMT1 loss (Chen et al., 2007; Milutinovic et al., 2004, 2003; Unterberger et al., 2006). It is possible that the hemi-methylated DNA that accumulates in dividing cells that lack Uhrf1 mimics damaged DNA and thus activates the DNA damage checkpoint. However, DNA damage typically blocks replication to prevent propagation of mutated DNA and to allow DNA repair. Indeed, topoisomerase 2a mutants have DNA damage and reduced cell proliferation (Dovey et al., 2009), and we found these mutants had very little BrdU incorporation (not shown), which is unlike the increase in DNA replication in *uhrf1* and *dnmt1* mutants. Other studies have reported that DNMT1 depletion from cancer cells causes an acute cell cycle arrest in S-phase (Milutinovic et al., 2003; Unterberger et al., 2006) and a recent study using *Xenopus* egg extracts shows a requirement for UHRF1 in origin licensing and processivity during DNA replication (Taylor et al., 2013). However, another study using *Xenopus* showed that UHRF1 depletion had no effect on DNA replication, but instead showed that blocking DNA replication abolished DNA methylation (Nishiyama et al., 2013). The difference between these and our findings may reflect the lack of checkpoints (in *Xenopus* extracts) or defective checkpoints (in cancer cells), compared with the checkpoint-enabled cells in embryos or there may be additional mechanisms to restrict epigenetic damage that function in the context of a whole organism. Indeed, our finding of a higher number of hepatocytes undergoing DNA replication but no increase in BrdU incorporation in the eye of the same larvae suggests that tissue-specific responses to DNA hypomethylation may be at play. It is possible that the growth restriction could be most profound in cells with high replicative potential, as it would be beneficial for embryos to exert the most stringent restrictions on cells such as hepatocytes that have limitless regenerative capacity and thus have a large potential contribution to the organism.

Development (2015) 142, 510-521 doi:10.1242/dev.115980

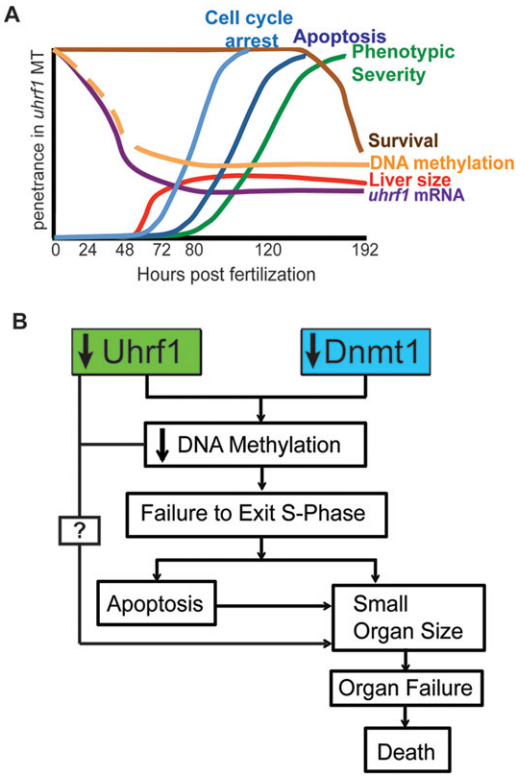

Fig. 8. Model of the relationship between *uhrf1* mutation, DNA methylation, cell cycle progression and hepatic outgrowth. (A) The temporal sequence of events in *uhrf1* mutants: *uhrf1* transcript loss is followed by DNA hypomethylation, cell cycle arrest, apoptosis, small liver size and larval lethality. (B) Uhrf1 and Dnmt1 loss lead to DNA hypomethylation, cell-cycle arrest and apoptosis to restrict organ outgrowth and cause lethality.

In summary, this work provides the first mechanistic understanding of how the loss of Uhrf1 and Dnmt1 lead to embryonic lethality and highlights a novel cellular response to methylome disruption. We believe our results from developing embryos can be extrapolated to other contexts where cells simultaneously experience epigenetic damage and a strong mitogenic stimulus. In these cases, cells may undergo futile cycles of DNA replication as a stop-gap measure to correct the methylome damage rather than transmit faulty epigenetic information to the next generation of cells that will populate the organism.

MATERIALS AND METHODS

Zebrafish maintenance, generation of transgenics and genotyping

Adult zebrafish were maintained on a 14:10 h light:dark cycle at 28°C in accordance with the policies of the Mount Sinai Institutional Animal Care and Use Committee. The *uhrf1*^{hi272} allele (abbreviated to *uhrf1* throughout) has been previously described (Sadler et al., 2007). *Tg(fabp10:UHRF1-GFP)Low* (Mudbhary et al., 2014) and *Tg (hsp70I:UHRF1-EGFP)* (Chu et al., 2012) were crossed to *uhrf1*$^{hi272+/-}$ fish. Embryos were heat shocked in pre-warmed water at 37°C for 50 min as described previously (Chu et al., 2012). Embryos were sorted for GFP expression within 4 h of heat shock; only the brightest embryos were assessed for liver size on 5 dpf. *Dnmt1*^{s904} mutants (Anderson et al., 2009) were obtained from M. Goll (Memorial Sloan-Kettering Cancer Center, New York, USA). *Tg(fabp10:dsRed)* fish (Dong et al., 2007) were obtained from D. Stainier.

Embryos from at least three clutches were individually genotyped at stages before mutants could be distinguished based on morphological phenotype (24-48 hpf). Tails from individual embryos were cut and transferred to DNA lysis buffer (10 mM Tris, 50 mM KCl, 0.3% Tween, 0.3% NP-40) and genotyped using primers in supplementary material Table S6. Heads were transferred to TRIZOL for RNA isolation or to genomic DNA lysis buffer for slot blotting, and 3-10 heads from the same genotype were pooled for RNA or DNA extraction.

Liver size and hepatocyte DNA content measurement

CY3-streptavadin (CY3-SA) labeling left liver lobe area measurements were carried out as described previously (Mudbhary et al., 2014). Embryos fixed in 4% paraformaldehyde were incubated in 50 µM solution of Sytox Green, washed with PBS and livers were dissected and imaged using confocal microscopy. Fluorescence intensity was measured with ImageJ. To account for the fact that a larger nuclear area might lead to more loosely distributed nucleic acid, we multiplied the average fluorescence of the nucleus by the area as a measure of total DNA content. Details of nuclear and hepatocyte size measurements can be found in the methods in the supplementary material.

DNA methylation analysis

Levels of 5-MeC were analyzed in total genomic DNA as described previously (Mudbhary et al., 2014).

RNA isolation and qPCR

RNA was extracted and cDNA was prepared for qPCR analysis as described previously (Mudbhary et al., 2014) using primers listed in supplementary material Table S6.

Nucleotide incorporation

10 mM BrdU or 100 µM EdU or a combination of both were used as indicated. Higher concentrations of EdU were lethal to *uhrf1* mutants. After BrdU/EdU wash, embryos were either fixed immediately in 4% PFA and processed for immunofluorescence or chased in embryo water.

Immunodetection

Embryos were homogenized by sonication and separated on 8-12% SDS gels, transferred to nitrocellulose and blotted with antibodies to DNMT1 (1:500, Santa Cruz, sc-20701), PCNA (1:500, Sigma, p8825), MCM3 (1:500, Bethyl Labs, A300-192A), pH3 (1:3000, Santa Cruz, sc-8656-R), UHRF1 (1:500, BD Biosciences, 611264), tubulin (1:5000, Developmental Studies Hybridoma Bank), AcH3 (1:3000, Millipore, 06-599), or H3K9me3 (1:3000, Abcam, ab-8898).

Immunofluorescence was carried out as described previously (Mudbhary et al., 2014) using antibodies against BrdU (1:200, BD Biosciences, 347580), histone H3 (1:200, Sigma, H0164), 5MeC (1:500, Eurogentec, BI-MECY-0100) and DNMT1 (1:10, Santa Cruz, sc-20701). Immunofluorescence for EdU was carried out following BrdU detection using Click-IT Alexa 488 Imaging Kit (Molecular Probes). After washing with PBST, embryos were incubated in either anti-rabbit Alexa 555 or Alexa 488 (1:500; Invitrogen) in 10% FBS in PBST. Nuclei were stained with Hoechst 33342 and imaged using a Leica SP5 DM confocal microscope. Whole fish were imaged using a SMZ1500 fluorescent microscope, and fluorescence quantification was carried out with ImageJ. For any assays where livers were imaged, a dorsal incision was made before immunofluorescence so that the liver was exposed but still attached to the fish. After immunofluorescence, livers were dissected and mounted in methylcellulose before imaging.

Cell death staining

The TUNEL assay was performed before BrdU staining according to the instructions provided in the In Situ Cell Death Detection Kit, TMR red (Roche), with embryos permeabilized with 10 µg/ml Proteinase K PBST prior to labeling. Larvae were incubated in 10 mg/ml Acridine Orange (Sigma) for 30 min in egg water and then rinsed before imaging with a SMZ1500 fluorescent microscope. Quantification of intensity was performed using the 'mean gray value' function in ImageJ.

Morpholino injections

Dnmt1 morpholino (5′-ACAATGAGGTCTTGGTAGGCATTTC-3) obtained from Gene Tools was diluted in RNase-free water to a 1 mM stock. On average, 4 nl of 0.05 mM stock of the *dnmt1* morpholino were injected into embryos prior to the four-cell stage.

Development (2015) 142, 510-521 doi:10.1242/dev.115980

Gene expression profiling

Genome-wide expression profiling was performed by using Zebrafish Genome Array (Affymetrix) according to manufacturer's instruction. Scanned raw data were normalized by using robust multiarray analysis (RMA) algorithm implemented in GenePattern genomic analysis toolkit (www.broadinstitute.org/genepattern) (Reich et al., 2006). Multiple probes corresponding to a single gene were collapsed into official gene symbol provided by NCBI by extracting a probe with maximal variation. Orthologous conversion to human genes was performed based on the mapping table provided by Zebrafish Model Organism Database (ZFIN, http://zfin.org). Differentially expressed genes were determined by using Bayesian *t*-test implemented in Cyber-T software (http://cybert.microarray.ics.uci.edu/) for top 1000 genes with the largest coefficient of variation. Posterior Probability of Differential Expression (PPDE) >0.95 was regarded as statistically significant. Induced or suppressed molecular pathways were determined by using Gene Set Enrichment Analysis (GSEA) (Subramanian et al., 2005) implemented in GenePattern genomic analysis toolkit (www.broadinstitute.org/genepattern) and Molecular Signature Database (MSigDB, http://www.broadinstitute.org/gsea/msigdb/index.jsp). False Discovery Rate (FDR) <0.25 was regarded as statistically significant.

Statistics

Standard deviation was calculated using MS Excel. Either an unpaired or paired one tailed Student's *t*-test or the Mann-Whitney *U*-test were used to determine *P*-values, except for survival curves, which used the log rank test.

Accession numbers

Data from the microarray was deposited in NCBI Gene Expression Omnibus with accession number GSE55339.

Acknowledgements

We are grateful to Evan Closser for expert fish care; to Raksha Mudbhary and Smita Gopinath for microarray analysis; to Mahip Grewal and Chi Zhang for technical support; and to Drs Walsh, Cassacia, Gouan-Evans and Ukomadu, and members of the Sadler lab for helpful discussions and suggestions on the manuscript.

Competing interests

The authors declare no competing financial interests.

Author contributions

V.J., Y.C. and K.C.S. conceived of the experiments. V.J., Y.C. and B.K. performed all experiments. P.S.T., X.C. and Y.H. performed microarray analysis. V.J. and K.C.S. wrote the manuscript.

Funding

This work was supported by grants from the National Institutes of Health [5R01DK080789 to K.C.S., R01DK099558 to Y.H., F30DK094503 to V.J. and T32CA078207-14 to support Y.C.] and the European Commission Framework Programme 7 [Heptromic, proposal number 259744 to Y.H.]. Deposited in PMC for release after 12 months.

Supplementary material

Supplementary material available online at
http://dev.biologists.org/lookup/suppl/doi:10.1242/dev.115980/-/DC1

References

Achour, M., Fuhrmann, G., Alhosin, M., Rondé, P., Chataigneau, T., Mousli, M., Schini-Kerth, V. B. and Bronner, C. (2009). UHRF1 recruits the histone acetyltransferase Tip60 and controls its expression and activity. *Biochem. Biophys. Res. Commun.* **390**, 523-528.

Amsterdam, A., Nissen, R. M., Sun, Z., Swindell, E. C., Farrington, S. and Hopkins, N. (2004). Identification of 315 genes essential for early zebrafish development. *Proc. Natl. Acad. Sci. USA* **101**, 12792-12797.

Anderson, R. M., Bosch, J. A., Goll, M. G., Hesselson, D., Dong, P. D. S., Shin, D., Chi, N. C., Shin, C. H., Schlegel, A., Halpern, M. et al. (2009). Loss of Dnmt1 catalytic activity reveals multiple roles for DNA methylation during pancreas development and regeneration. *Dev. Biol.* **334**, 213-223.

Arima, Y., Hirota, T., Bronner, C., Mousli, M., Fujiwara, T., Niwa, S.-i., Ishikawa, H. and Saya, H. (2004). Down-regulation of nuclear protein ICBP90 by p53/p21Cip1/WAF1-dependent DNA-damage checkpoint signals contributes to cell cycle arrest at G1/S transition. *Genes Cells* **9**, 131-142.

Arita, K., Ariyoshi, M., Tochio, H., Nakamura, Y. and Shirakawa, M. (2008). Recognition of hemi-methylated DNA by the SRA protein UHRF1 by a base-flipping mechanism. *Nature* **455**, 818-821.

Avvakumov, G. V., Walker, J. R., Xue, S., Li, Y., Duan, S., Bronner, C., Arrowsmith, C. H. and Dhe-Paganon, S. (2008). Structural basis for recognition of hemi-methylated DNA by the SRA domain of human UHRF1. *Nature* **455**, 822-825.

Bashtrykov, P., Jankevicius, G., Jurkowska, R. Z., Ragozin, S. and Jeltsch, A. (2014). The UHRF1 protein stimulates the activity and specificity of the maintenance DNA methyltransferase DNMT1 by an allosteric mechanism. *J. Biol. Chem.* **289**, 4106-4115.

Berkyurek, A. C., Suetake, I., Arita, K., Takeshita, K., Nakagawa, A., Shirakawa, M. and Tajima, S. (2014). The DNA methyltransferase Dnmt1 directly interacts with the SET and RING finger-associated (SRA) domain of the multifunctional protein Uhrf1 to facilitate accession of the catalytic center to hemi-methylated DNA. *J. Biol. Chem.* **289**, 379-386.

Biniszkiewicz, D., Gribnau, J., Ramsahoye, B., Gaudet, F., Eggan, K., Humpherys, D., Mastrangelo, M.-A., Jun, Z., Walter, J. and Jaenisch, R. (2002). Dnmt1 overexpression causes genomic hypermethylation, loss of imprinting, and embryonic lethality. *Mol. Cell. Biol.* **22**, 2124-2135.

Bostick, M., Kim, J. K., Esteve, P.-O., Clark, A., Pradhan, S. and Jacobsen, S. E. (2007). UHRF1 plays a role in maintaining DNA methylation in mammalian cells. *Science* **317**, 1760-1764.

Chen, T., Hevi, S., Gay, F., Tsujimoto, N., He, T., Zhang, B., Ueda, Y. and Li, E. (2007). Complete inactivation of DNMT1 leads to mitotic catastrophe in human cancer cells. *Nat. Genet.* **39**, 391-396.

Cheng, J., Yang, Y., Fang, J., Xiao, J., Zhu, T., Chen, F., Wang, P., Li, Z., Yang, H. and Xu, Y. (2013). Structural insight into coordinated recognition of trimethylated histone H3 lysine 9 (H3K9me3) by the plant homeodomain (PHD) and tandem tudor domain (TTD) of UHRF1 (ubiquitin-like, containing PHD and RING finger domains, 1) protein. *J. Biol. Chem.* **288**, 1329-1339.

Chu, J., Loughlin, E. A., Gaur, N. A., SenBanerjee, S., Jacob, V., Monson, C., Kent, B., Oranu, A., Ding, Y., Ukomadu, C. et al. (2012). UHRF1 phosphorylation by cyclin A2/cyclin-dependent kinase 2 is required for zebrafish embryogenesis. *Mol. Biol. Cell* **23**, 59-70.

Dong, P. D. S., Munson, C. A., Norton, W., Crosnier, C., Pan, X., Gong, Z., Neumann, C. J. and Stainier, D. Y. R. (2007). Fgf10 regulates hepatopancreatic ductal system patterning and differentiation. *Nat. Genet.* **39**, 397-402.

Dorn, E. S. and Cook, J. G. (2011). Nucleosomes in the neighborhood: new roles for chromatin modifications in replication origin control. *Epigenetics* **6**, 552-559.

Dovey, M., Patton, E. E., Bowman, T., North, T., Goessling, W., Zhou, Y. and Zon, L. I. (2009). Topoisomerase II alpha is required for embryonic development and liver regeneration in zebrafish. *Mol. Cell. Biol.* **29**, 3746-3753.

Du, Z., Song, J., Wang, Y., Zhao, Y., Guda, K., Yang, S., Kao, H.-Y., Xu, Y., Willis, J., Markowitz, S. D. et al. (2010). DNMT1 stability is regulated by proteins coordinating deubiquitination and acetylation-driven ubiquitination. *Sci. Signal.* **3**, ra80.

Feng, S., Cokus, S. J., Zhang, X., Chen, P.-Y., Bostick, M., Goll, M. G., Hetzel, J., Jain, J., Strauss, S. H., Halpern, M. E. et al. (2010). Conservation and divergence of methylation patterning in plants and animals. *Proc. Natl. Acad. Sci. USA* **107**, 8689-8694.

Hashimoto, H., Horton, J. R., Zhang, X., Bostick, M., Jacobsen, S. E. and Cheng, X. (2008). The SRA domain of UHRF1 flips 5-methylcytosine out of the DNA helix. *Nature* **455**, 826-829.

Hervouet, E., Lalier, L., Debien, E., Cheray, M., Geairon, A., Rogniaux, H., Loussouarn, D., Martin, S. A., Vallette, F. M. and Cartron, P.-F. (2010). Disruption of Dnmt1/PCNA/UHRF1 interactions promotes tumorigenesis from human and mice glial cells. *PLoS ONE* **5**, e11333.

Hopfner, R., Mousli, M., Oudet, P. and Bronner, C. (2002). Overexpression of ICBP90, a novel CCAAT-binding protein, overcomes cell contact inhibition by forcing topoisomerase II alpha expression. *Anticancer Res.* **22**, 3165-3170.

Jacob, Y., Stroud, H., LeBlanc, C., Feng, S., Zhuo, L., Caro, E., Hassel, C., Gutierrez, C., Michaels, S. D. and Jacobsen, S. E. (2010). Regulation of heterochromatic DNA replication by histone H3 lysine 27 methyltransferases. *Nature* **466**, 987-991.

Jegu, T., Latrasse, D., Delarue, M., Mazubert, C., Bourge, M., Hudik, E., Blanchet, S., Soler, M.-N., Charon, C., De Veylder, L. et al. (2013). Multiple functions of Kip-related protein5 connect endoreduplication and cell elongation. *Plant Physiol.* **161**, 1694-1705.

Karpf, A. R. and Matsui, S.-i. (2005). Genetic disruption of cytosine DNA methyltransferase enzymes induces chromosomal instability in human cancer cells. *Cancer Res.* **65**, 8635-8639.

Kim, J. K., Esteve, P.-O., Jacobsen, S. E. and Pradhan, S. (2009). UHRF1 binds G9a and participates in p21 transcriptional regulation in mammalian cells. *Nucleic Acids Res.* **37**, 493-505.

Li, X., Meng, Q., Rosen, E. M. and Fan, S. (2011). UHRF1 confers radioresistance to human breast cancer cells. *Int. J. Radiat. Biol.* **87**, 263-273.

Milutinovic, S., Zhuang, Q., Niveleau, A. and Szyf, M. (2003). Epigenomic stress response: knockdown of DNA methyltransferase 1 triggers an intra-S-phase arrest of DNA replication and induction of stress response genes. *J. Biol. Chem.* **278**, 14985-14995.

Milutinovic, S., Brown, S. E., Zhuang, Q. and Szyf, M. (2004). DNA methyltransferase 1 knock down induces gene expression by a mechanism independent of DNA methylation and histone deacetylation. *J. Biol. Chem.* **279**, 27915-27927.

Mistry, H., Tamblyn, L., Butt, H., Sisgoreo, D., Gracias, A., Larin, M., Gopalakrishnan, K., Hande, M. P. and McPherson, J. P. (2010). UHRF1 is a genome caretaker that facilitates the DNA damage response to gamma-irradiation. *Genome Integr.* **1**, 7.

Mudbhary, R. and Sadler, K. C. (2011). Epigenetics, development, and cancer: zebrafish make their mark. *Birth Defects Res. C Embryo Today* **93**, 194-203.

Mudbhary, R., Hoshida, Y., Chernyavskaya, Y., Jacob, V., Villanueva, N., Fiel, M. I., Chen, X., Kojima, K., Thung, S., Bronson, R. T. et al. (2014). UHRF1 overexpression drives DNA hypomethylation and hepatocellular carcinoma. *Cancer Cell* **25**, 196-209.

Muto, M., Kanari, Y., Kubo, E., Takabe, T., Kurihara, T., Fujimori, A. and Tatsumi, K. (2002). Targeted disruption of Np95 gene renders murine embryonic stem cells hypersensitive to DNA damaging agents and DNA replication blocks. *J. Biol. Chem.* **277**, 34549-34555.

Nishiyama, A., Yamaguchi, L., Sharif, J., Johmura, Y., Kawamura, T., Nakanishi, K., Shimamura, S., Arita, K., Kodama, T., Ishikawa, F. et al. (2013). Uhrf1-dependent H3K23 ubiquitylation couples maintenance DNA methylation and replication. *Nature* **502**, 249-253.

Obata, Y., Furusawa, Y., Endo, T. A., Sharif, J., Takahashi, D., Atarashi, K., Nakayama, M., Onawa, S., Fujimura, Y., Takahashi, M. et al. (2014). The epigenetic regulator Uhrf1 facilitates the proliferation and maturation of colonic regulatory T cells. *Nat. Immunol.* **15**, 571-579.

Papait, R., Pistore, C., Grazini, U., Babbio, F., Cogliati, S., Pecoraro, D., Brino, L., Morand, A.-L., Dechampesme, A.-M., Spada, F. et al. (2008). The PHD domain of Np95 (mUHRF1) is involved in large-scale reorganization of pericentromeric heterochromatin. *Mol. Biol. Cell* **19**, 3554-3563.

Qian, C., Li, S., Jakoncic, J., Zeng, L., Walsh, M. J. and Zhou, M.-M. (2008). Structure and hemimethylated CpG binding of the SRA domain from human UHRF1. *J. Biol. Chem.* **283**, 34490-34494.

Qin, W., Leonhardt, H. and Spada, F. (2011). Usp7 and Uhrf1 control ubiquitination and stability of the maintenance DNA methyltransferase Dnmt1. *J. Cell. Biochem.* **112**, 439-444.

Reich, M., Liefeld, T., Gould, J., Lerner, J., Tamayo, P. and Mesirov, J. P. (2006). GenePattern 2.0. *Nat. Genet.* **38**, 500-501.

Rottach, A., Frauer, C., Pichler, G., Bonapace, I. M., Spada, F. and Leonhardt, H. (2010). The multi-domain protein Np95 connects DNA methylation and histone modification. *Nucleic Acids Res.* **38**, 1796-1804.

Sadler, K. C., Krahn, K. N., Gaur, N. A. and Ukomadu, C. (2007). Liver growth in the embryo and during liver regeneration in zebrafish requires the cell cycle regulator, uhrf1. *Proc. Natl. Acad. Sci. USA* **104**, 1570-1575.

Sharif, J., Muto, M., Takebayashi, S.-i., Suetake, I., Iwamatsu, A., Endo, T. A., Shinga, J., Mizutani-Koseki, Y., Toyoda, T., Okamura, K. et al. (2007). The SRA protein Np95 mediates epigenetic inheritance by recruiting Dnmt1 to methylated DNA. *Nature* **450**, 908-912.

Stroud, H., Hale, C. J., Feng, S., Caro, E., Jacob, Y., Michaels, S. D. and Jacobsen, S. E. (2012). DNA methyltransferases are required to induce heterochromatic re-replication in Arabidopsis. *PLoS Genet.* **8**, e1002808.

Subramanian, A., Tamayo, P., Mootha, V. K., Mukherjee, S., Ebert, B. L., Gillette, M. A., Paulovich, A., Pomeroy, S. L., Golub, T. R., Lander, E. S. et al. (2005). Gene set enrichment analysis: a knowledge-based approach for interpreting genome-wide expression profiles. *Proc. Natl. Acad. Sci. USA* **102**, 15545-15550.

Taylor, E. M., Bonsu, N. M., Price, R. J. and Lindsay, H. D. (2013). Depletion of Uhrf1 inhibits chromosomal DNA replication in Xenopus egg extracts. *Nucleic Acids Res.* **41**, 7725-7737.

Tien, A. L., Senbanerjee, S., Kulkarni, A., Mudbhary, R., Goudreau, B., Ganesan, S., Sadler, K. C. and Ukomadu, C. (2011). UHRF1 depletion causes a G2/M arrest, activation of DNA damage response and apoptosis. *Biochem. J.* **435**, 175-185.

Tittle, R. K., Sze, R., Ng, A., Nuckels, R. J., Swartz, M. E., Anderson, R. M., Bosch, J., Stainier, D. Y. R., Eberhart, J. K. and Gross, J. M. (2011). Uhrf1 and Dnmt1 are required for development and maintenance of the zebrafish lens. *Dev. Biol.* **350**, 50-63.

Truong, L. N. and Wu, X. (2011). Prevention of DNA re-replication in eukaryotic cells. *J. Mol. Cell Biol.* **3**, 13-22.

Unoki, M., Nishidate, T. and Nakamura, Y. (2004). ICBP90, an E2F-1 target, recruits HDAC1 and binds to methyl-CpG through its SRA domain. *Oncogene* **23**, 7601-7610.

Unterberger, A., Andrews, S. D., Weaver, I. C. G. and Szyf, M. (2006). DNA methyltransferase 1 knockdown activates a replication stress checkpoint. *Mol. Cell. Biol.* **26**, 7575-7586.

Vijayaraghavalu, S., Dermawan, J. K., Cheriyath, V. and Labhasetwar, V. (2013). Highly synergistic effect of sequential treatment with epigenetic and anticancer drugs to overcome drug resistance in breast cancer cells is mediated via activation of p21 gene expression leading to G2/M cycle arrest. *Mol. Pharm.* **10**, 337-352.

Xie, S., Jakoncic, J. and Qian, C. (2012). UHRF1 double tudor domain and the adjacent PHD finger act together to recognize K9me3-containing histone H3 tail. *J. Mol. Biol.* **415**, 318-328.

Supplementary Materials and Methods

Nuclear and hepatocyte size measurements

Area of nuclei and hepatocytes from confocal sections of *uhrf1* mutant and WT larvae expressing membrane localized GFP (*Tg(fabp10:CAAX-GFP*)) was calculated with ImageJ. Measurement for both characteristics were obtained from cells in the same livers but they were not correlated so that it was not possible to generate individual cell-by-cell measurements. Instead, the nuclear size and the cell size was averaged for all WT and mutant hepatocytes and the ratio of these was compared.

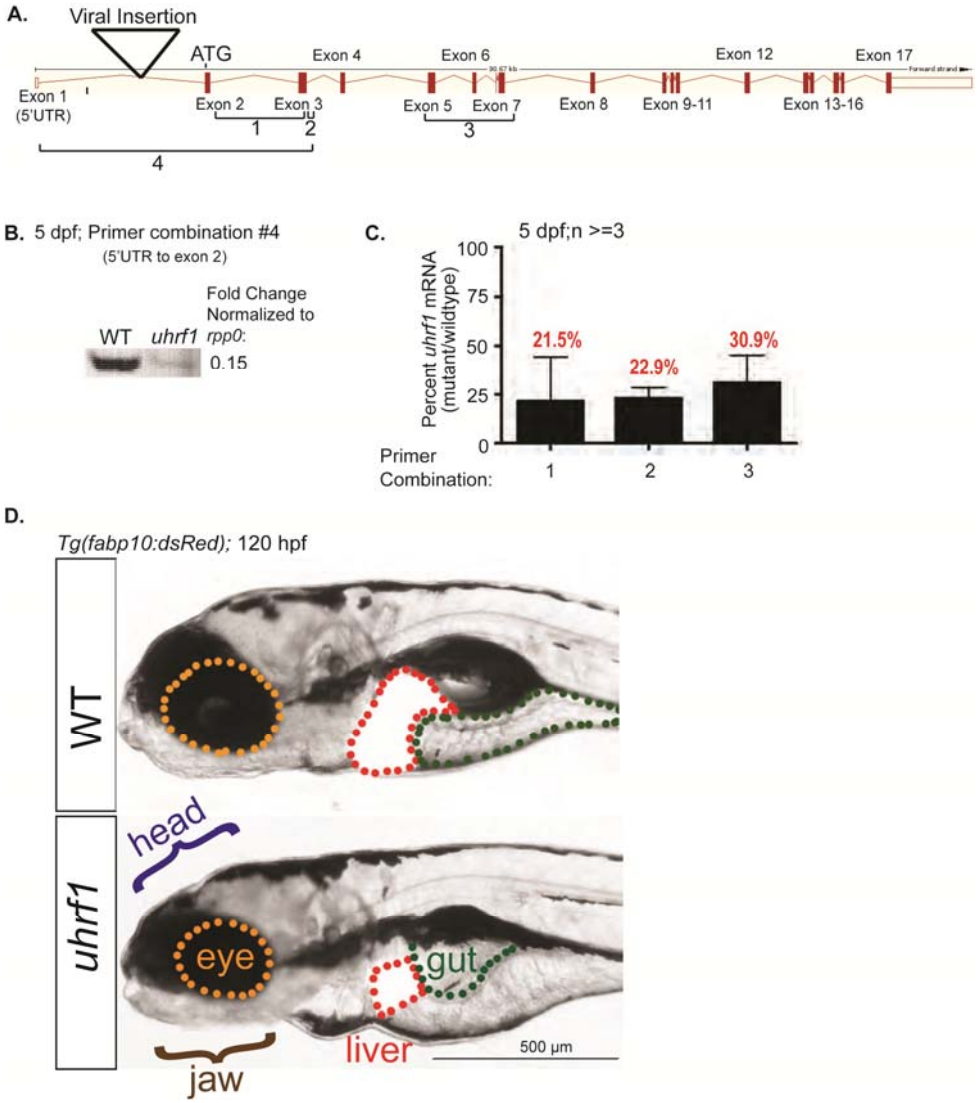

Figure S1. The *uhrf1*^{hi272} allele is a hypomorphic mutation.

(A) Location of viral insertion in the *uhrf1* gene along with primers to regions amplified to determine transcript expression. (B) Agarose gel run with contents of qPCR reaction using primers from 5'UTR to Exon 2 in 5 dpf *uhrf1* mutant and wild type larvae. (C) qPCR for *uhrf1* in 5 dpf mutant fish relative to WT using primers indicated in A. (D) WT and uhrf1 larvae at 120 hpf expressing the *fabp10:dsRed* transgene (liver highlighted in white). The most severely affected structures are annotated on the mutant

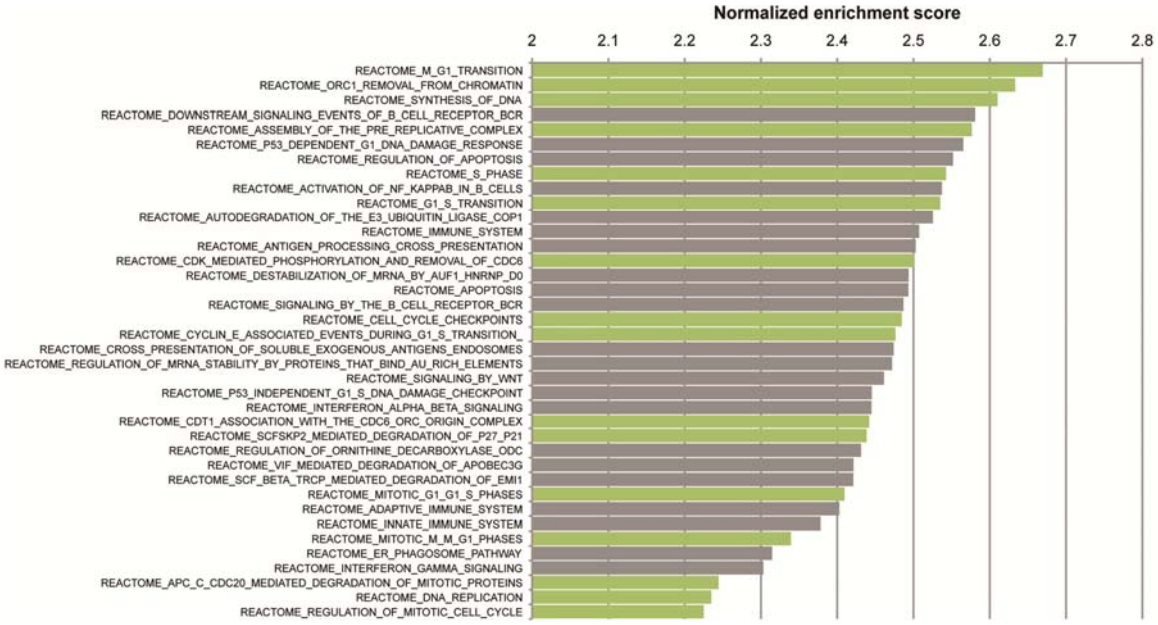

Figure S2. Microarray of *uhrf1* mutants shows enrichment of gene sets relevant to cell cycle control.

Normalized enrichment scores of the Reactome pathways identified by Gene Set Enrichment Analysis. Cell cycle relevant pathways are in green.

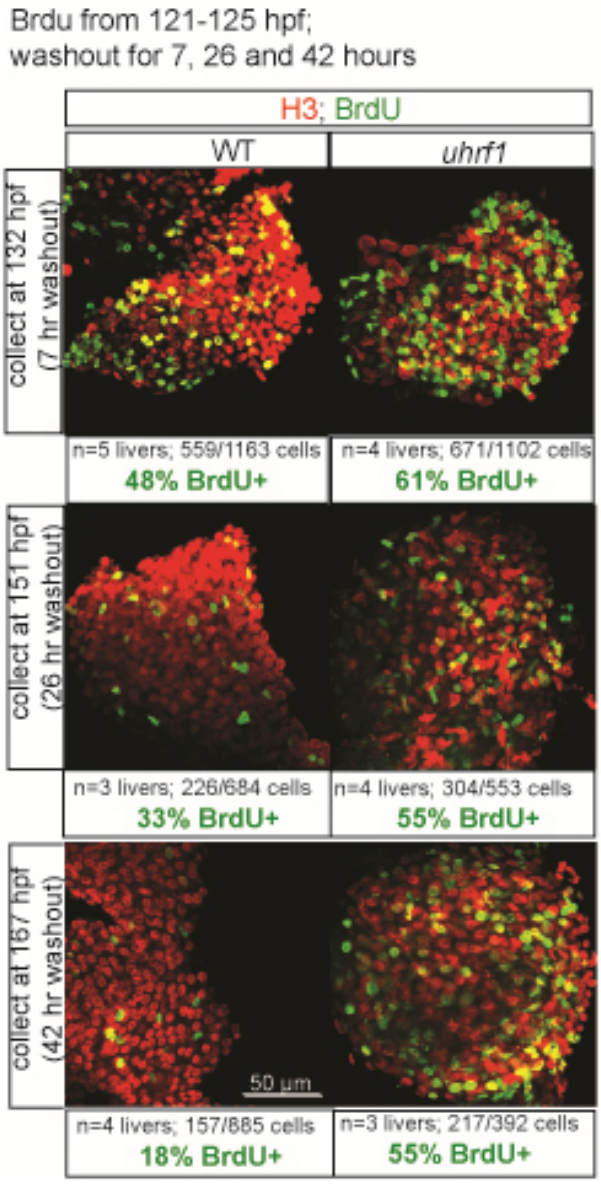

Figure S3. Nuclear size is increased in *uhrf1* mutants.

Confocal z-stacks through whole livers from larvae labeled with BrdU as outlined in Figure 3A. BrdU positive cells (green) were counted and taken as a percent of total nuclei, counterstained with anti-hisone H3 (red).

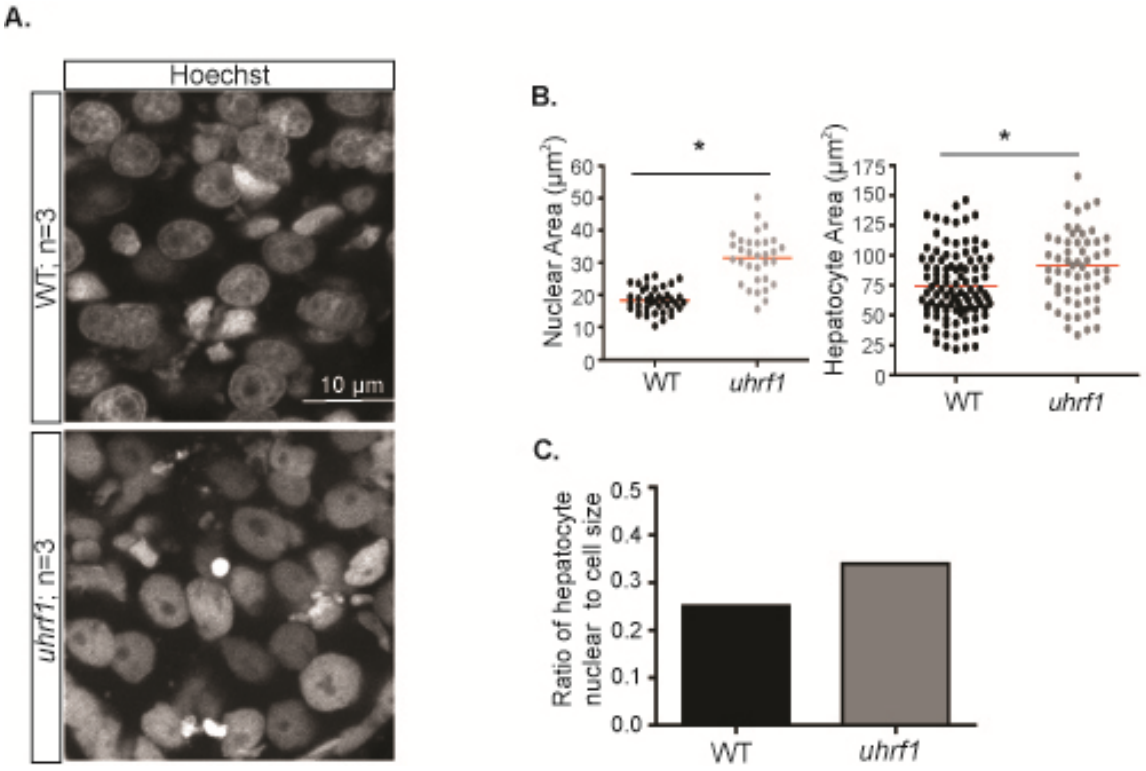

Figure S4. The nucleus is disproportionately enlarged in *uhrf1* mutant hepatocytes.

(A) Nuclear morphology of hepatocytes were visualized by Hoechst staining in 5 dpf *uhrf1* and WT larvae. (B) Hepatocyte area was quantified by outlining the cell periphery using membrane localized GFP as a guide in *Tg(fabp10:CAAX-GFP)* fish and the nuclear size was quantified based on Hoechst staining. Each dot represents a single hepatocyte from at least 2 individual larvae. (C) The nuclear:cell size ratio was determined for hepatocyes by dividing the average area of the nucleus to the average area of the hepatocyte from the data shown in (B). Both measurements were not consistently obtained from the same cells and therefore the average for each cellular feature over multiple cells was compared. This illustrates that although both nuclei and the total hepatocyte size is increased in *uhrf1* mutants, the nuclei are disproportionately larger.

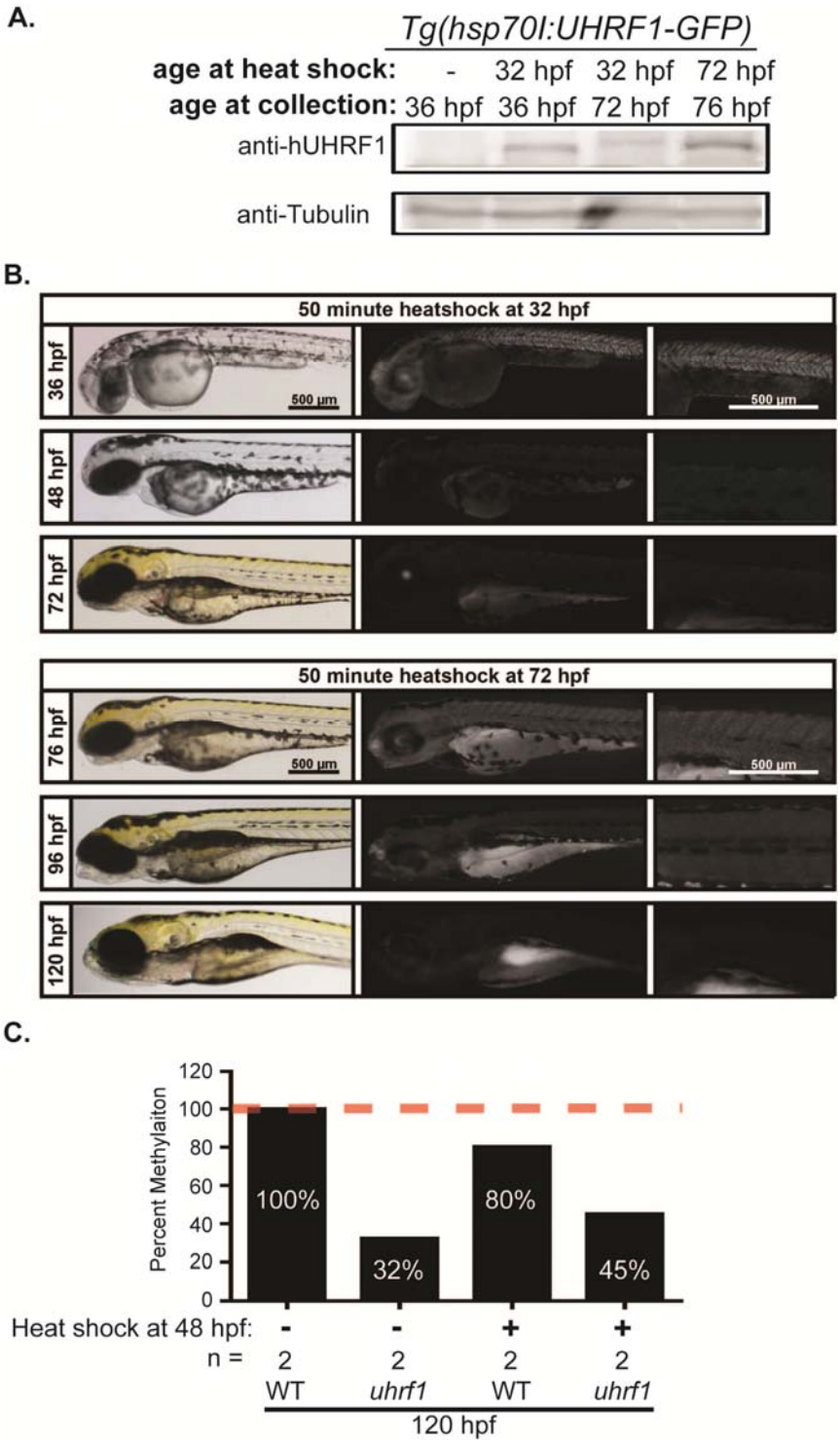

Figure S5. Heat shock induces transient expression of UHRF1-GFP.

Tg(hsp70l:hUHRF1-GFP) embryos were heat shocked at 37° C for 45 minutes at 48 hpf and collected over a time course for Western blot (A) or imaging (B) to detect transgene expression. (A) Western blot for human UHRF1 (hUHRF1) and tubulin as a loading control in embryos collected at the indicated times after heat shock at 48 hpf.

(B) Length of recombinant protein persistence after heat shock as assessed by GFP fluorescence in whole larvae at the time points indicated. (C) Average percent of 5-MeC in 120 hpf (5 dpf) larvae with and without heat shock at 48 hpf, as determined by slot blot analysis in two independent clutches.

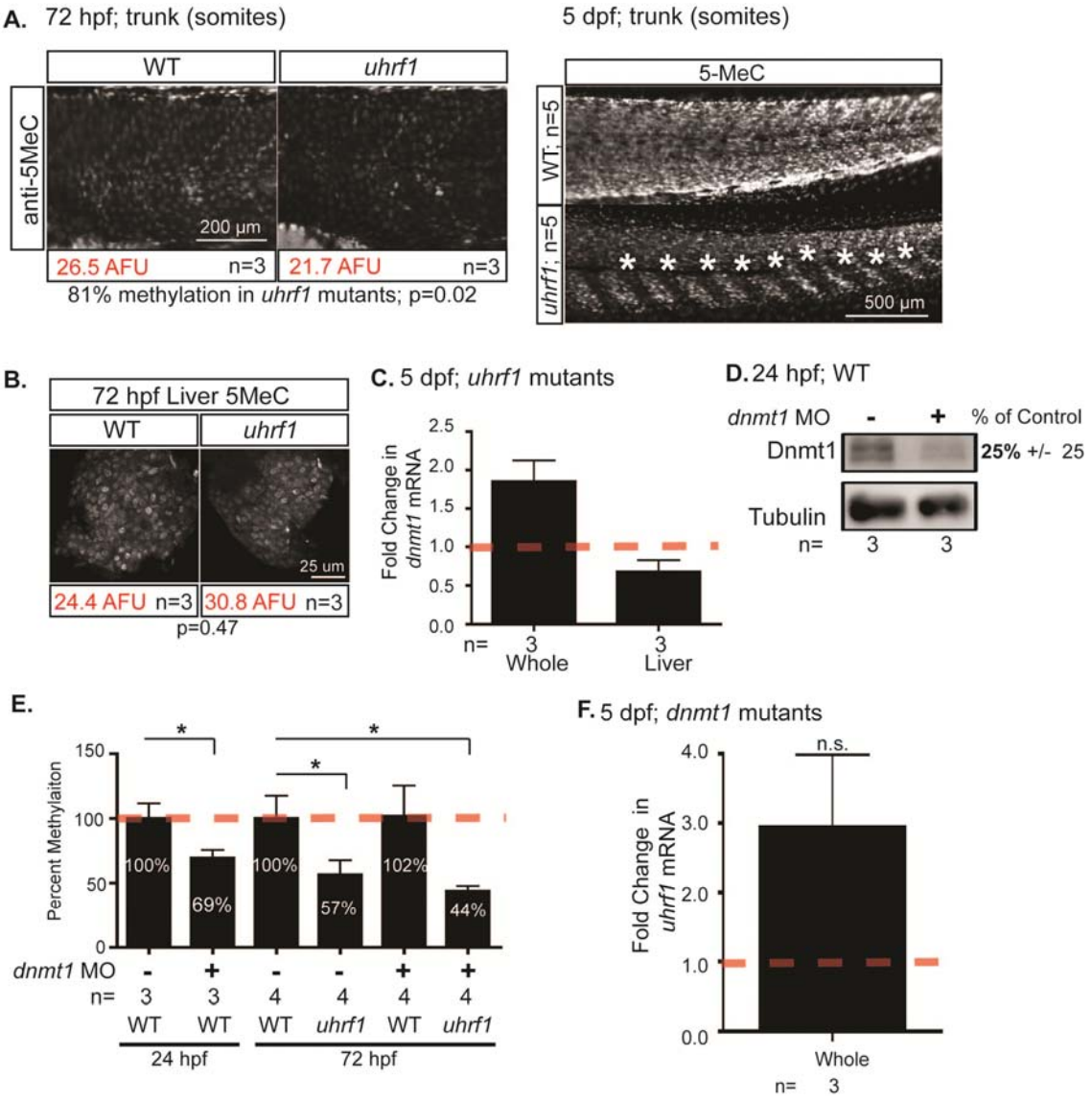

Figure S6. DNA methylation is reduced in *uhrf1* mutants and *dnmt1* morphants.

(A) 5-MeC immunofluorescence in posterior trunk of WT and *uhrf1* embryos at 72 hpf (left) and 5dpf (right). Fluorescent intensity was calculated for the 72 hpf samples based on arbitrary fluorescence units (AFU) in the intra-somitic regions and the average for 3 embryos is indicated. DNA methylation was reduced by 19% in *uhrf1* mutants, p value was determined by a 1-sample t-test. (B) Hepatic 5-MeC levels were calculated in the liver of 72 hpf *uhrf1* mutants and phenotypically WT siblings as in

(A) and the average fluorescence from 3 embryos is indicated (n=3). There is no significant difference in fluorescence between these samples by a 1-sampled t-test. (C) *dnmt1* mRNA expression was determined by qPCR in 5 dpf WT and *uhrf1* whole embryos and dissected livers and expressed as average fold change relative to WT levels. (D) *dnmt1* MO injection reduced Dnmt1 protein as assayed by Western Blot. (E) *dnmt1* morpholino injection reduces DNA methylation in 24 hpf WT embryos and in 72 hpf *uhrf1* mutants. 5-MeC levels determined by slot-blotting were normalized to total DNA levels. Percent methylation in *dnmt1* morphants was determined by normalizing to control embryos. p values were determined by a 1-sampled t-test relative to the age matched WT controls and * indicates p value < 0.04. (F) *uhrf1* mRNA expression was measured by qPCR in whole 5 dpf WT and *dnmt1* mutants.

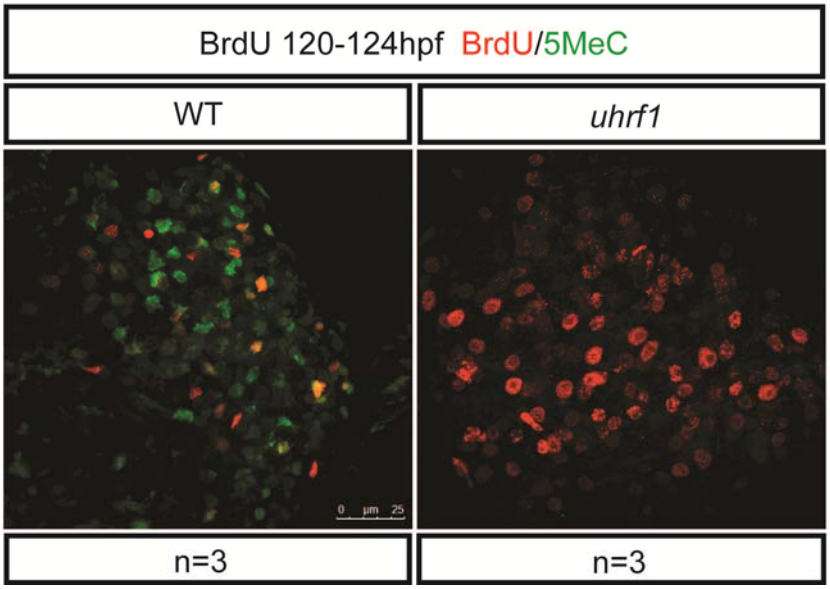

Figure S7. BrdU is incorporated into hepatocytes with low DNA methylation. Immunofluorescence for 5-MeC (green) and BrdU (red) on WT and *uhrf1* mutant livers of larvae treated from 120-124 hpf with 10 mM BrdU. Representative of 5 individual experiments.

Table S1

Click here to Download Table S1

Table S2

Click here to Download Table S2

Table S3

Click here to Download Table S3

Table S4

Click here to Download Table S4

Table S5

Click here to Download Table S5

Table S6. Primers used for PCR and quantitative real-time PCR

Gene Name	*Primer Name*	Sequence 5'-3'
uhrf1 (for genotyping *uhrf1*^{hi272} mutant)	*272geneF*	ggtttgtccattttggaagc
	272geneR	ttcccgagaagaagataacagg
	MSL4	gctagcttgccaaacctacaggt
cyclin A2 [Danio rerio]	*ccna2-Fq1*	gattgcgatcccttcctcaa
	ccna2-Rq1	cgggtagatcctccaaagagtaacccg
cyclin D1 [Danio rerio]	*ccnd1-Fq1*	ctgtgcgacagacgtcaact
	ccnd1-Rq1	ggtgaggttctgggatgaga
cyclin E1 [Danio rerio]	*ccne1-Fq1*	cgatttagccagtccagcagaatcg
	ccne1-Rq1	gctgggcaagcaaagatgaagt
cell division cycle 45 [Danio rerio]	*cdc45-Fq1*	cccacagacctgttgatgtg
	cdc45-Rq1	ccatctgcttcttcgtcctc
cell division cycle 6 [Danio rerio]	*cdc6-Fq1*	agcaggcgacaggtctaaaa
	cdc6-Rq1	gctctcgccatctccactac
minichromosome maintenance complex component 2 [Danio rerio]	*mcm2-Fq1*	ctgtgcgtcacatcgagtct
	mcm2-Rq1	gaacttctgcgtgtcgatga
minichromosome maintenance complex component 3 [Danio rerio]	*mcm3-Fq1*	catggagcgcgcaaatacaccg
	mcm3-Rq1	ttcggtctccaggtttcacg
minichromosome maintenance complex component 4 [Danio rerio]	*mcm4-Fq1*	cgagaagccctgaaacagtc
	mcm4-Rq1	cacttcctccttacgcttgc
origin recognition complex subunit 3 [Danio rerio]	*orc3-Fq1*	acaagtgaaatccccacagc
	orc3-Rq1	gtgcttcacagctgcacat
origin recognition complex subunit 6 [Danio rerio]	*orc6-Fq1*	cctcttcatctggagccaag
	orc6-Rq1	tgcctcttttgagtgccttt
polymerase (DNA directed), alpha 1, catalytic subunit [Danio rerio]	*pola1-Fq1*	agaagatggaggaggggaaa
	pola1-Rq1	caggaacaccactccaggtt

polymerase (DNA directed), delta 1, catalytic subunit [Danio rerio]	*pold1-Fq1*	cagcacaggagtatgcagga
	pold1-Rq1	aactccctttgctgctttga
proliferating cell nuclear antigen [Danio rerio]	*pcna-Fq1*	atggcgtgaagttctctgct
	pcna-Rq1	tgcactggctcattcatctc
uhrf1 [Danio rerio]	*zuhrf1-5-utr*	catcttctgttcccgagagg
	zuhrf1-Fq1	atgtggattcaggtgcgcactatg
	zuhrf1-Rq1	gaccatcctccatctgtttgcc
	zuhrf1-Fq2	acgacatcgttcagctgttg
	zuhrf1-Rq2	tcgatgaggtctgctgtgtc
	zuhrf1-Fq3	cgacatggcctttcacacctac
	zuhrf1-Rq3	cggagtctcctttagcttctctccg